Universidad de La Laguna

Initiation to the theoretical study of materials: DFT for C, Si, Ge and Sn

Submitted by

Álvaro Monforte Marín

TFG Advisors

Dra. Silvana Elena Radescu Cioranescu
Dr. Andrés Mujica Fernaud

A Final Degree Work submitted to the University of La Laguna in partial fulfillment of the requirement for the degree of Grado en Física

Academic Course 2021-2022

Abstract

Grado en Física

**Initiation to the theoretical study of materials:
DFT for C, Si, Ge and Sn**

by **Álvaro Monforte Marín**

The study of condensed matter is one of the main fields in modern Physics. A few years ago, was divided into two streams: "hard" condensed matter physics, which studies quantum properties of matter, and "soft" condensed matter physics which studies those properties of matter for which quantum mechanics plays no role. Central to this field is to understand how electrons and nuclei interact according to the well-established laws of electromagnetism and quantum mechanics, and try to explain their properties.

The complexity of the computational calculus is insanely huge. Nowadays it is normal to understand this field as something collaborative between different groups of researchers in order to have access, not only to more human resources but also to hardware or software that allows in some way or another to reduce this computational cost. The ab initio theories and calculations try to access physical-mathematical routes that shorten these in an analytical way and also nourished by an empirical support to offer the best possible approximations.

The present work will be focused in an introductory background of these ab initio calculations that will support our understanding of how they will applied to study different materials, in both diamond structures, cubic and hexagonal (called lonsdaleite) for C (Carbon), Si (Silicon), Ge (Germanium) and Sn (Tin). The program used will be VASP (Vienna ab initio Simulation Package). Convergence studies, Equations of States with Birch-Murnaghan approximation, Density of States, band structure and phonon frequencies will be studied.

The results obtained are consistent with current published calculations and theories, thus confirming to the reproducibility and consistency of the results. Therefore, they will be compared with publications extracted from different sources (the most used one is Arxiv).

The diamond structure appears in different materials. It has beautiful optical properties and a very high thermal conductivity (Carbon). Still, the hexagonal form of diamond (it was observed for the first time in meteorite craters [1]), could now be produced e.g. under shock compression experiments [2], and is significantly stiffer and stronger than regular gem diamonds. The understanding of the differences between them could give us a key for the next step in the discovering new materials.

Acknowledgements

Antes de comenzar el trabajo me gustaria agradecer a mis tutores la Dra. Silvana Elena Radescu Cioranescu y el Dr. Andrés Mujica Fernaud por sus contribuciones a este trabajo, me han ayudado a entender y desarrollar este manuscrito.

Muchas gracias a mis padres, Joaquina y Jesús, y mi hermana Alicia por todo lo que han contribuido, apoyado y formado a lo largo de toda mi vida. Muchas gracias por acompañarme en cualquiera de las dimensiones de mi persona posibles a Steven, Eduardo, Mario y Sara; además, de todos mis amigxs en general.

Y muchas gracias a mi pareja Fátima, que me ha apoyado inexorablemente desde el cariño y el aprecio, entendido y comprendido, con una mano tendida cuando me puse piedras en el camino.

Soy un mero transeúnte de mi realidad circundante y ellxs la han hecho mas bella.

Contents

List of Figures

List of Tables

Chapter 1

Theoretical Background

1.1 Introduction

The objective of this chapter is to introduce from first principles certain notions, functions and theorems that allow us to obtain the Kohn-Sham equations. For this we will show the Born-Oppenheimer Hamiltonian, establishing a problem that will be solved with the DFT theory. Which rests on the two Hohenberg-Kohn Theorems, where we will make use of the variational principle. We will show the way to solve the problem of V-representability and N-representability, with the Levi-Lieb functional.

It is continued with the obtaining of the kohn sham equations, also obtaining its representation in crystalline momentum basis. At the same time presenting and mentioning their range of performance of both the LDA and GGA approximations.

It will end with the pseudo potential theory, the Hellmann-Feynman force equations and the derivation of the birch-murnaghan approximation.

1.2 Born-Oppenheimer Approximation

We can understand solids as densely packed atoms characterized by structural rigidity. The relevance of the high number of particles that compose it cannot be treated equally, we can propose the paradigm of treating this ensemble as an union of an inert subset regarding the aggregate state of the system and another subset that will play a central role in the field of the study of condensed matter and chemistry, such as the electronic valence layer. Both interact with each other, they are not decoupled. This mindset will help us to interpret the following equations.

We need to solve the equation that allows us to understand the system, the time-independent Schrödinger equation $\hat{H}\psi = E\psi$ where ψ describes the state of the system, in which the Hamiltonian operator that governs it has the following structure:

$$\hat{H} = \underbrace{\hat{T}_e + \hat{V}_{ee}}_{\hat{H}_e} + \underbrace{\hat{T}_n + \hat{V}_{nn}}_{\hat{H}_n} + \underbrace{\hat{V}_{en}}_{\hat{H}_{int}} \tag{1.1}$$

The non-relativistic Hamiltonian of a system of electrons {coordinates $\mathbf{r}_i$, momenta $\hat{\mathbf{p}}_i$, charge e } and nuclei {coordinates $\mathbf{R}_i$, momenta $\hat{\mathbf{P}}_i$, charge $+Z_I e$ } is composed of different parts:

- The electronic hamiltonian:

$$\hat{H}_e = \sum_i \frac{\hat{\mathbf{p}}_i^2}{2m} + \frac{1}{2}\frac{e^2}{4\pi\epsilon_0}\sum_{i\neq j}\frac{1}{|\mathbf{r_i}-\mathbf{r_j}|} \tag{1.2}$$

- The nuclei hamiltionian:

$$\hat{H}_n = \sum_I \frac{\hat{\mathbf{p}}_I^2}{2M_I} + \frac{1}{2}\frac{e^2}{4\pi\epsilon_0}\sum_{I\neq J}\frac{Z_I Z_J}{|\mathbf{R_I}-\mathbf{R_J}|} \tag{1.3}$$

- The electron-nuclei interaction hamiltonian:

$$\hat{H}_{int} = -\frac{e^2}{4\pi\epsilon_0}\sum_I \frac{z_I}{|\mathbf{r}-\mathbf{R_I}|} \tag{1.4}$$

The different terms we appreciate in these expressions are (in order from left to right): in (1.2) the kinetic energy of electrons and the electric potential energy the electron-electron term, in (1.3) the kinetic energy of nucleous and the electric potential energy nuclei-nuclei term, finally in (1.4) the electric potential energy electron-nuclei term.

The Born-Oppenheimer approach is based on the assumption that we can decouple the motion of the nucleus of the electronic cloud. Due to two ideas: one is that the mass of the nucleus as a rule is of the order of 10^3 times greater than that of the electrons. Being under the influence of the forces such as the Coulomb interaction, the acceleration of these bodies is inversely proportional to their masses.

Electrons react to any effect instantaneously, so we can understand nuclei as fixed points in space. Finally we can entablish the electronic wavefunction depends upon the nuclear positions but not upon their velocities. the other is that the nuclear motion (e.g., rotation, vibration) sees a smeared out potential from the speedy electrons.

Now we can drop the kinetic energy of the nuclei term from our Hamiltonian and we can work without the electric potential energy nuclei-nuclei because is constant for every single fixed configuration (carefully with that bias in the future). Now we have as new hamiltonian of Born-Oppenheimer (BO), where we have an electronic part and interaction between "the cloud" and the nuclei:

$$\hat{H}_{BO} \implies \hat{H} = \hat{H}_e + \hat{H}_{int} \tag{1.5}$$

The wavefunctions ψ depends on the position and spins of the N electrons. we will not deal with the spin, so we can neglect it.

$$\psi(\mathbf{r}_1, \mathbf{r}_2, ..., \mathbf{r}_N;\ \underbrace{\mathbf{R}_1, \mathbf{R}_2, ..., \mathbf{R}_N}_{\text{Parametric dependence}}\ ) \tag{1.6}$$

$$\rho(\mathbf{r}) = \rho(\mathbf{r}; \mathbf{R}_1, \mathbf{R}_2, ..., \mathbf{R}_N) \tag{1.7}$$

$$E = E(\mathbf{R}_1, \mathbf{R}_2, ..., \mathbf{R}_N) \tag{1.8}$$

Problematic

Even with the Born-Oppenheimer approximatoon, the many-body wave function (1.6) still is a complicated object, to find the ground state we must solve a multidimensional Schrödinger equation where the potential for each particle depends of each others.

$$\psi(\mathbf{r}_1, ..., \mathbf{r}_n; \mathbf{R}_1, ..., \mathbf{R}_n) = \langle \mathbf{r}_1, ..., \mathbf{r}_n; \mathbf{R}_1, ..., \mathbf{R}_n | \psi \rangle \tag{1.9}$$

$$\hat{H}|\psi\rangle = E|\psi\rangle \tag{1.10}$$

The computational methods to solve this, using the via of discretization; e.g. if we have M states to be occupied and N fermionic particles with spin up and spin down, the Hilbert space ℓ size will be:

$$dim\{\ell\} = \left(\frac{M!}{(M - \frac{n}{2})!(\frac{n}{2})!} \right)^2 \Bigg|_{M=200, N=100} \sim 10^{95}$$

1.3 Density Functional Theory, DFT

1.3.1 Introduction

The birth of the density functional theory germinates with an idea belonging to the theory of Thomas and Fermi. Their started semi-classical approach to be applicable is the spatial variations of the de Broglie wavelength, the system in question must be small. Like Kohn said in his nobel lecture [3]: "However the theory had one feature which interested me", not only the idea of electrons moving in a external potential, also the a provided one-to-one correspondence between $v(\mathbf{r})$ and $\rho(\mathbf{r})$.

The theory is usefull in terms of obtaining the total energy of ions but it has a problem, that is expressed in terms of $\rho(\mathbf{r})$ and Schrödinger theory is in terms of $\psi(\mathbf{r}_1, \mathbf{r}_2, ..., \mathbf{r}_N)$, so is difficult to entablished a relation between them.

Walter Kohn in his noble Lecture [3], suggested that in the past he had an example in mind that led him to determine an hypothesis that considerates the starting point of the modern Density Funcional Theory: *"a knowledge of the groundstate density of $n(\mathbf{r})$ for any electronic system , (with of without interactions) uniquely determines the system."*.

Kohn mentions other important consideration about other idea that motives him to take a second step, the proposal of Hartree with his equations he shows the paradigm of calculations to solve the self-consistent equations.

Hartree show a simple idea, electrons move in a effective single particle coulombic potential, after optimized the system respect the spatial component of the space and

with the non-interaction approach he got a Schrödinger-like equation to solve with a self-consistent method.

These are the Hartree equations:

$$(-\frac{\hbar}{2m}\nabla^2 + v_{eff}(\mathbf{r}))\phi_i(\mathbf{r})) = \epsilon\phi_i(\mathbf{r}),\ j = 1, ..., N \tag{1.11}$$

$$\rho(\mathbf{r}) = \sum_i^N |\phi_i(\mathbf{r})|^2 \tag{1.12}$$

With the self-consistent scheme:

$$\rho(\mathbf{r})^{(0)} \implies \underbrace{v_{eff}(\mathbf{r})}_{v_{Hartree}} \implies \underbrace{(1.11)}_{\text{respect}\,\phi_i(\mathbf{r})} \implies \rho(\mathbf{r})^{(1)} \tag{1.13}$$

Is a bit different of Thomas-Fermi theory, not only in the Kinetic term also in the single particle aproximation fo the density. It calculates much better the ground state, this is the seed that will take in mind for the use of Hartree-like equations (1.11) (1.12), and then improving them.

The Density Functional Theory reformulates the problem to be able to obtain, for example, the energy and electronic distribution of the ground state, working with the electron density functional instead of the wave function. One advantage is that the density is a much simpler quantity than the wave function and therefore easier to calculate, in practice much more complex systems are accessible: the wave function of a system of N electrons depends on 3N variables, while the electron density only depends on 3 variables.

1.3.2 The density $\rho(\mathbf{r})$ as the basic variable

Consider a wave function dependent on spin and spatial coordinates:

$$\rho(\mathbf{r}) = \langle\psi|\hat{\rho}(\mathbf{r})|\psi\rangle = N \sum_{spin} \int d\mathbf{r}_2 ... d\mathbf{r}_N |\psi(\mathbf{r}_1, ..., \mathbf{r}_n)|^2 \tag{1.14}$$

$$N = \int d\mathbf{r}\rho(\mathbf{r}) \tag{1.15}$$

In detail, the integral in the equation gives the probability that a particular electron with arbitrary spin is found in the volume element $d\mathbf{r}_1$. Due to the fact that the electrons are indistinguishable, N times the integral gives the probability that any electron is found there.

The other electrons represented by the wave function $\psi(\mathbf{r}_1, ..., \mathbf{r}_n)$ have arbitrary spin and spatial coordinates. If additionally the spin coordinates are neglected, the electron density can even be expressed as measurable observable only dependent on spatial coordinates.

How can we be sure that a certain density is really the ground state density that we are looking for?

1.3.3 Hohenberg-Kohn theorems

Theorem 1 (Variational Principle) *Given any normalized function ψ' (that satisfies the appropriate boundary conditions), then the expectation value of the Hamiltonian represents an upper bound to the exact ground state energy.*

$$\langle \psi' | \hat{H} | \psi' \rangle \geq E_0 \tag{1.16}$$

So-called Rayleigh-Ritz approximation is essential like method to solve with a trial function a group of self-consistency equations. Also provides to Hohenberg and Kohn a tool to reformulate the wavefunction dependence like Hartree did to show the key of the knowledge of groundstate. Where E_0 is the lowest energy, associated to the groundstate. One thing that we can not forget is that Rayleigh-Ritz minimization principle can be generalized to ensembles of unequally weighted states. It can help us in a future amplification of the physical theorical results of this work.

Theorem 2 (1^{st} Hohenberg-Kohn Theorem) *[4] The groundstate density $\rho(\mathbf{r})$ of a bound system of interacting electrons in some external potential $v(\mathbf{r})$, determines this potential uniquely. In other words, the existence of a duality between the ground-state density and the external potential, univocally relates both (neglecting a possible additive constant).*

Proof:

The proof proceeds by *reductio ad absurdum*. This Lemma provides us with an external potential that, in this demonstration, we denote as $v(\mathbf{r})$, so this method consists of assuming the existence of another external potential $v'(\mathbf{r})$ with it schrödinger equation assoctiated as we can show in the next table:

$E = \langle \psi^{(G)} \vert \hat{H} \vert \psi^{(G)} \rangle$	$E' = \langle \psi'^{(G)} \vert \hat{H}' \vert \psi'^{(G)} \rangle$
$\hat{H}$	$\hat{H}'$
$\psi^{(G)}$	$\psi'^{(G)}$
$v(\mathbf{r})$	$v'(\mathbf{r})$
E	E'

TABLE 1.1: Scheme of the proof of the 1^{st} Hohenberg-Kohn Theorem

The key is that the new hamiltonian has a ground state $\psi'^{(G)}$ with the same particle density $\rho(\mathbf{r})$ as the ground state $\psi^{(G)}$. So applying the minimal property of the ground state (this is the variational principle (1)) we find:

Note: $\psi'^{(G)}$ cannot be equal to $\psi^{(G)}$ at least $(v'(\mathbf{r}) - v(\mathbf{r})) = 0$

$$E' = \langle \psi'^{(G)} | \hat{H}' | \psi'^{(G)} \rangle < \langle \psi^{(G)} | \hat{H}' | \psi^{(G)} \rangle = \langle \psi^{(G)} | \hat{H} + \hat{V}' - \hat{V} | \psi^{(G)} \rangle \tag{1.17}$$

$$E' < \langle \psi^{(G)} | \hat{H}' | \psi^{(G)} \rangle + \langle \psi^{(G)} | \hat{V}' | \psi^{(G)} \rangle - \langle \psi^{(G)} | \hat{V} | \psi^{(G)} \rangle \tag{1.18}$$

$$E' < E + \int \big(v'(\mathbf{r}) - v(\mathbf{r}) \big) \rho(\mathbf{r}) d\mathbf{r} \tag{1.19}$$

Likewise for E:

$$E < \langle \psi'^{(G)} | \hat{H} | \psi'^{(G)} \rangle + \langle \psi'^{(G)} | \hat{V} | \psi'^{(G)} \rangle - \langle \psi'^{(G)} | \hat{V}' | \psi'^{(G)} \rangle \tag{1.20}$$

$$E < E' + \int \big(v(\mathbf{r}) - v'(\mathbf{r}) \big) \rho(\mathbf{r}) d\mathbf{r} \tag{1.21}$$

We arrive into an inconsistency:

$$E + E' < E + E' \tag{1.22}$$

The external potencial $v(\mathbf{r})$ is uniquely determined (up to a constant) by $\rho(\mathbf{r})$, the ground state density.

Theorem 3 (2^{nd} Hohenberg-Kohn Theorem) *[4] A universal functional for the energy $E[\rho]$ can be defined in terms of the density. The exact ground state is the global minimum value of this functional.*

Proof:

Electrons moving in an external potential, can be study by a Hamiltonian like:

$$\hat{H} = \underbrace{\hat{T} + \hat{V}_{ee}}_{\hat{H}_e} + \underbrace{\sum_{i=1}^{N} \hat{v}_{ext}(i)}_{\hat{H}_{int} = \hat{V}_{ext}} \tag{1.23}$$

The density variable ρ can describe the ground state as we saw in the first Hohenber-Kohn Theorem (2). A density that is the ground-state of some external potential is known as v-representable. Following from this, a v-representable energy functional $E_v[\rho(\mathbf{r})]$ can be defined in which the external potential $v_{ext}(\mathbf{r})$ is unrelated to another density $\rho'(\mathbf{r})$, so we can create an energy functional $E_0[\rho]$ in this way:

$$E[\rho] = T[\rho] + V_{ee}[\rho] + \int v_{ext}(\mathbf{r}) \rho(\mathbf{r}) d^3\mathbf{r} \tag{1.24}$$

Also, we can consider another energy functional $E[\rho']$:

$$E[\rho'] = T[\rho'] + V_{ee}[\rho'] + \int v_{ext}(\mathbf{r}) \rho'(\mathbf{r}) d^3\mathbf{r} \tag{1.25}$$

Applying the Rayleigh-Ritz variational principle (1), a different density, it will necessarily give a higher energy:

$$E_0 = E[\rho]_0 = \langle \psi^{(G)} | \hat{H} | \psi^{(G)} \rangle < \langle \psi^{(1)} | \hat{H} | \psi'^{(1)} \rangle = E[\rho']_1 = E_1 \tag{1.26}$$

Where E_0 is the energy of the ground state $\psi^{(G)}$ (the lowest), E_1 other energy associted to state $\psi^{(1)}$ with density $\rho'(\mathbf{r})$. So the mean value of the hamiltonian $\hat{H}$ respect $\psi^{(1)}$ will have more energy than the ground state as we saw.

There are two kinds of problems. We talk about densities but they are linked to the external potential, which is unknown. The well-known v-representability problem. Hohenberg and Kohn didnt show us a way to treat with it. On the other hand, we didnt treat the degenerate case of the ground states. we will deal with both problems in the next subsection.

1.3.4 V-representability problem and N-representability

Further, the Hohenberg-Kohn functional does not tell us if the density that minimizes the energy functional gives us back a true physical quantity, i.e. that the resulting density originates from an antisymmetric many-body wave function corresponding to the ground-state of an arbitrary local external potential. Both conditions are the so-called N-representability and V-representability condition.

In other form, How do I know, given an arbitrary function $\rho(\mathbf{r})$, that it is a density coming from an antisymmetric N-body wave function? How do I know, given an arbitrary function $\rho(\mathbf{r})$, that it is the ground state density of a local potential v(r). In its original formulation, the Hohenberg-Kohn theorems were restricted to pure-state V-representable densities.

The essence of usual DFT calculations is to replace the interacting system by a much simpler auxiliary non-interacting one, i.e. the Kohn-Sham approach. It solely works if a non-interacting potential exists that reproduces the density of the interacting system, i.e. the non-interacting V-representability condition. We cannot forget the antisymmetric restriction. For the electron density the N-representability problem is solved [5], since any non-negative, differentiable, normalized function can be written in terms of some antisymmetric wave function, and therefore is N-representable. In the next subsection I will present a procedure that verifies only N-representable densities.

1.3.5 Levy-Lieb constrained search

We applicate a step-wise minimization procedure, assuming the N-representable densities as a subset of the V-representable. Let define the set of normalized antisymmetric wavefunctions with finite energy:

$$W_N = \left\{ \psi \in H_N \mid \langle \psi | \psi \rangle = 1, \langle \psi | \hat{T} | \psi \rangle < \infty \right\} \tag{1.27}$$

N-representability of the densites[a]:

$$\left\{ \rho \mid \exists \psi \in W_N \implies \rho_\psi = \rho \right\} \tag{1.28}$$

When we talk about finite energy of electrons our task is to assume $\int |\nabla \sqrt{n(\mathbf{r})}|^2 d\mathbf{r}$. We use a trial density $\tilde{\rho}$ that belongs to W_N and $W_N \in R_N$ (all posible V-represensatable and N-representable densities). In terms fo the Variational Principle (1) and using theorem (3) we have[b]:

$$E_0 = \min_{\psi \in W_N} \{ \langle \psi | H_N | \psi \rangle \} = \min_{\tilde{\rho} \in R_N} \left\{ \min_{\psi \in W_N | \tilde{\rho}_\psi = \tilde{\rho}} \{ \langle \psi | H_N | \psi \rangle \} \right\} \tag{1.29}$$

Where $\psi \in W_N | \tilde{\rho}_\psi = \tilde{\rho}$ means that the trial ρ belongs to W_N and will be minimized in R_N.

$$\min_{\tilde{\rho} \in R_N} \left\{ \min_{\psi \in W_N | \tilde{\rho}_\psi = \tilde{\rho}} \left\{ \langle \psi[\tilde{\rho}] | [\hat{T} + \hat{V}_{ee} | \psi[\tilde{\rho}] \rangle + \int V_{ext}(\mathbf{r}) \rho(\mathbf{r}) d^3 r \right\} \right\} \tag{1.30}$$

$$\min_{\tilde{\rho} \in R_N} \left\{ \min_{\psi \in W_N | \tilde{\rho}_\psi = \tilde{\rho}} \left\{ \langle \psi[\tilde{\rho}] | [\hat{T} + \hat{V}_{ee} | \psi[\tilde{\rho}] \rangle \right\} + \int V_{ext}(\mathbf{r}) \tilde{\rho}(\mathbf{r}) d^3 r \right\} \tag{1.31}$$

Where we have the so-called Levy-Lieb Functional:

$$F_{LL}[\rho] = \min_{\psi \in W_N | \tilde{\rho}_\psi = \tilde{\rho}} \left\{ \langle \psi[\tilde{\rho}] | [\hat{T} + \hat{V}_{ee} | \psi[\tilde{\rho}] \rangle \right\} \tag{1.32}$$

Of course, we assume that the arbitrary trial density can be obtained from an antisymmetric wavefunction, in other words, is N-representable.

So finally,

$$E_0 = \min_{\tilde{\rho} \in R_N} \left\{ F_{LL} + \int V_{ext}(\mathbf{r}) \tilde{\rho}(\mathbf{r}) d^3 r \right\} \tag{1.33}$$

$$E_0 = \min_{\tilde{\rho}} \left\{ \underbrace{\min_{\psi \to \tilde{\rho}} \{ \langle \psi[\tilde{\rho}] | [\hat{T} + \hat{V}_{ee} | \psi[\tilde{\rho}] \rangle \}}_{F_{LL}[\tilde{\rho}]} + \int V_{ext}(\mathbf{r}) \tilde{\rho}(\mathbf{r}) d^3 r \right\} \tag{1.34}$$

[a] Levy showed that one could consider all N-representable densities in such a search, instead of searching in the smaller (and nearly impossible to define) space of v-representable densities.

[b] Lieb showed that the ground state can always be found by applying the variational principle to Levy's formulation of DFT. His work also discusses more mathematical aspects.

Where $F_{LL}[\rho]$ searches for the minimum of the expectation value of kinetic energy plus $\hat{V}_{ee}$ interaction operator over the domain of all N-representable wave function.

The outer minimization further restricts the domain to the set of densities that integrate to the particle number of the system (V-representable).

1.3.6 Kohn-Sham Equations

We apply Kohn-Sham approach, that consider non-interacting electrons aproximating it with a product of spatial and spin component (with a degenerate of two, up and down), obeying the spin coordinate we get:

$$\rho(\mathbf{r}) = \sum_{i}^{occupied} |\phi_i(\mathbf{r})|^2 = \sum_{i}^{occupied} \phi_i(\mathbf{r})\phi_i^*(\mathbf{r}) \tag{1.35}$$

Taking into account that the density of the ground state has the property of uniqueness, we can consider an arbitrary non-interacting system that has the same density as the interacting system. That is the reason of the powerful of Kohn-Sham approach.

For N interacting electrons, we have a Functional $F[\tilde{\rho}(\mathbf{r})]$ Hohenberg-Kohn like that respect the Levy-Lieb constrained search formulated in terms of a trial density $\tilde{\rho}$.

$$F[\tilde{\rho}(\mathbf{r})] \equiv T_{non}[\tilde{\rho}(\mathbf{r})] + \underbrace{\frac{1}{2}\frac{e^2}{4\pi\epsilon_0}\int \frac{\tilde{\rho}(\mathbf{r})\tilde{\rho}'(\mathbf{r})}{|\mathbf{r}-\mathbf{r}'|}d\mathbf{r}d\mathbf{r}' + E_{xc}[\tilde{\rho}(\mathbf{r})]}_{\text{electrons interaction}} \tag{1.36}$$

Where we have $T_{non}[\rho(\mathbf{r})]$ that is the kinectic energy functional for non-interacting electrons, then the interacting terms: the 'Hartree' and the so-called exchange-correlation term is:

$$E_{exchange}[\rho] = (T[\rho] - T_{non}[\rho]) + (V_{ee}[\rho] - V_{Hartree}[\rho]) \tag{1.37}$$

Taking in mind (3) the Hohenberg-Kohn variational principle leads:

$$E[\tilde{\rho}; v_{ext}(\mathbf{r})] \equiv \underbrace{T_{non}[\tilde{\rho}] + V_{Hartree}[\tilde{\rho}] + E_{xc}[\tilde{\rho}]}_{F[\tilde{\rho}]} + \int v_{ext}(\mathbf{r})\tilde{\rho}(\mathbf{r})d\mathbf{r} \geq E^{(G)} \tag{1.38}$$

Where for each trial density, always the Energy will be higher than the ground-state.

Is well-known that the particle number N is positive quantity that constrained the system, letting us putting conditions for the minimization process, can be calculated by the expression:

$$N = \int \tilde{\rho}(\mathbf{r})d^3r = \int \tilde{\rho}d\mathbf{r} \tag{1.39}$$

We can apply the Lagrangian multiplier method assuming the restriction (1.39) and solving the optimization problem

$$\frac{\delta}{\delta\tilde{\rho}(\mathbf{r})}\left\{E[\tilde{\rho};v_{ext}(\mathbf{r})]-\mu\int\tilde{\rho}d\mathbf{r}\right\}\Big|_{\tilde{\rho}=\rho}=0\implies\frac{\delta E[\tilde{\rho};v_{ext}(\mathbf{r})]}{\delta\tilde{\rho}(\mathbf{r})}\Big|_{\tilde{\rho}=\rho}=\mu \tag{1.40}$$

We need to pay attention on the derivative of a funcional, is not exactly as the derivative of a function, is a quite a different, so we have the expression:

$$J[f+\delta f]-J[f]=\delta J[f]\equiv\int\underbrace{\frac{\delta J[f]}{\delta f(\mathbf{r})}}_{slope}\delta f(\mathbf{r})d\mathbf{r} \tag{1.41}$$

Derivating all summands of (1.38) respect to $\rho(\mathbf{r})$ and clearing the variable μ:

$$\left(\frac{\delta T_{non}[\rho]}{\delta\tilde{\rho}}+\underbrace{\frac{\delta V_{Hartree}[\rho]}{\delta\tilde{\rho}}+\frac{\delta E_{xc}[\rho]}{\delta\tilde{\rho}}+\frac{\delta E_{ext}}{\delta\tilde{\rho}}}_{v_eff}\right)\Bigg|_{\tilde{\rho}=\rho}=\mu \tag{1.42}$$

$$\left\{-\frac{\hbar^2}{2m}\nabla^2+v_{eff}[\rho](\mathbf{r})\right\}\phi_i(\mathbf{r})=\epsilon_i\phi_i(\mathbf{r}) \tag{1.43}$$

With charge density:

$$\rho(\mathbf{r})=\sum_n|\psi(\mathbf{r})|^2 \tag{1.44}$$

We can represent the different summands of the Hamiltonian in terms of the spatial components, after introduce (1.43) in a self-consistent process (remember that the external potential is the same in the continuum of the calculus and exchange-correlation term is approximated via some approach):

$$V_{Hartree}[\rho]=\frac{1}{2}\frac{e^2}{4\pi\epsilon_0}\sum_{ij}\langle\phi_i\phi_j|\frac{1}{r_{12}}|\phi_i\phi_j\rangle \tag{1.45}$$

$$T_{non}[\rho]=\sum_i\langle\phi_i|\left(-\frac{\hbar^2}{2m}\nabla^2\right)|\phi_i\rangle \tag{1.46}$$

The sum of the orbital energies is related to the total energy as:

$$E=\sum_i^N\epsilon_i-\frac{1}{2}\frac{e^2}{4\pi\epsilon_0}\sum_{ij}\langle\phi_i\phi_j|\frac{1}{r_{12}}|\phi_i\phi_j\rangle+E_{xc}[\rho]-\int V_{xc}(\mathbf{r})\rho(\mathbf{r})d\mathbf{r} \tag{1.47}$$

1.3.7 LDA: Local Density Approximation

Proposed by Kohn and Sham in [4] although in the Thomas-Fermi Theory <cite>, we could saw the seed. They consider a local approximation of the Kinetic Energy, treating it like an uniform electron gas.

The main variable $\rho(\mathbf{r})$ can show certain behaviour, depend of that we can use it to approximate our unknown term E_{xc}. If $\rho(\mathbf{r})$ varies slowly in the material, we can approximate the solid as an uniform gas.

In this approximation the exchange-correlation energy is the same as the hommogenous gas which is well-known, for example, Fermi used it in his paper proof.

$$E_{xc}^{(LDA)} = \int \rho(\mathbf{r}) \underbrace{\epsilon_{xc}(\rho(\mathbf{r}))}_{\text{Homogenous gas}} d\mathbf{r} \tag{1.48}$$

In the Kohn-Sham equations we use, like we did in the construction of the self-consistent equations:

$$v_{xc}(\mathbf{r}) = \frac{\delta E_{xc}^{(LDA)}}{\delta\rho(\mathbf{r})} = \epsilon_{xc}(\rho(\mathbf{r})) + \rho(\mathbf{r})\frac{d\epsilon_{xc}(\rho(\mathbf{r}))}{d\rho(\mathbf{r})} \tag{1.49}$$

In the LDA approximation the total groud-state energy $E^{(G;LDA)}$ has the form:

$$E^{(G;LDA)} = \sum_i \epsilon_i - \frac{1}{2}\frac{e^2}{4\pi\epsilon_0}\int \rho(\mathbf{r})\frac{1}{|\mathbf{r}-\mathbf{r}'|}\rho(\mathbf{r}')d\mathbf{r}d\mathbf{r}' - \int n(\mathbf{r})\frac{d\epsilon_{xc}(\rho(\mathbf{r}))}{d\rho(\mathbf{r})}\rho(\mathbf{r})d\mathbf{r} \tag{1.50}$$

The LDA approximation has to be adequate for system with a low spatial varying electron density, but it revealed good for a wider variety of materials. It, however, significantly fails in the description of many properties of d and f compounds. It presents a simple problem, is local that probably will show problems , we can improve it taking into account a more general case, at least in mathematical properties.

Electronic densities of atoms in the core region, where the electrons are quite localized, are poor with that approximation. The reason is that the LDA fails to cancel the self-interaction, which is important for strongly localized states. This point can punish the calculations of this work in the next section when we introduce the Pseudopotential method.

Main Limitations:

- Inhomogeneities in the density are not taken into account.
- The Hartree term presents a self-interaction, the LDA does not cancel this term.
- only local, non-local not incluided; also, there are problems with the strong local correlation effects[c].

[c] Problems to predict the bandgap of oxide metals such as Fe or Mn, predicting that they are semiconductors instead of insulators.

- In some cases, it does not predicts well the ground state, it does not take into account the Van der Waals bonding[d].

1.3.8 GGA: Generalized Gradient Approximation

One of the main limitation in the LDA was the inexistence of a inhomogenity treatment of the gas. In this case is useful to carry out a Taylor expansion of the density in terms of the gradient and higher derivatives. So normally we will have an integrand with a coefficient that depends on the density, the density and one of it is derivate:

$$E_{xc} = \int \underbrace{\rho(\mathbf{r})\epsilon_{xc}[\rho(\mathbf{r})]F_{xc}[\rho(\mathbf{r}), \nabla\rho(\mathbf{r}), \nabla^2\rho(\mathbf{r}), ...]}_{f(\rho(\mathbf{r}), |\nabla\rho(\mathbf{r})|, ...)} d\mathbf{r} \tag{1.51}$$

For example, as semi-local approximation that is a quite better than LDA, we can take the gradient part and cut the expansion as:

$$E_{xc}^{(GGA)} = \int f(\,\rho(\mathbf{r}), |\nabla\rho(\mathbf{r})|\,)\, d\mathbf{r} \tag{1.52}$$

Where $f\,(\rho(\mathbf{r}), |\nabla\rho(\mathbf{r})|)$ represents a function with the whole dependencies of the integrand. The zeroth order is the LDA, if we consider second order derivatives, we can talk about meta-GGA Method. The exact exchange-correlation energy is the electrostatic interaction between the electron density at a point and the density of the exchange-correlation hole surrounding an electron at that point. It possible to talk about the creation of the hole, considering three effects: self-interaction correction, pauli principle and coulomb repulsion. But in this work we will not talk about holes. One of the key points, they greatly reduce the bond dissociation energy error, and generally improve transition-state barriers. Many papers which studied the worthness of the using approximations like GGA and meta-GGA against LDA or anothers, like the study of [6] also in [7]. But, unlike LDA, there is no single universal form.

1.3.9 Kohn-Sham Equations in a crystalline momentum basis

The Kohn-Sham equations (1.43) for the crystal are:

$$\hat{h}_{KS}\,[\rho]\,|\phi_{n\mathbf{k}}\rangle = \left[\hat{t} + \hat{v}_{eff}\,[\rho]\right]|\phi_{n\mathbf{k}}\rangle = \epsilon_{n\mathbf{k}}|\phi_{n\mathbf{k}}\rangle \tag{1.53}$$

Where:

- The Kohm-Sham orbitals are (in position representation) :

$$\langle\mathbf{r}|\phi_{n\mathbf{k}}\rangle = \phi_{n,\mathbf{k}}(\mathbf{r}) = e^{i\mathbf{k}\mathbf{r}}u_{n,\mathbf{k}}(\mathbf{r}) \tag{1.54}$$

  The orbital functions are constructed by considering the Bloch theorem (4).

[d] The important case of the DNA, the Hidrogen bonding is essential in this structure, so LDA approximation would be a problem in this case, because it predicts stronger bonds.

- The charge density is:

$$\rho(\mathbf{r}) = \sum_{n\mathbf{k}}^{oc} |\phi_{n\mathbf{k}}(\mathbf{r})|^2 = \sum_{\mathbf{k}} \underbrace{\sum_{n}^{oc} |\phi_{n\mathbf{k}}(\mathbf{r})|^2}_{\rho_{\mathbf{k}}(r)} = \frac{\Omega_c}{(2\pi)^3} \int_{\Omega_{FBZ}} d\mathbf{k} |\rho_{\mathbf{nk}}(r)|^2 \tag{1.55}$$

  Where the sum in quantum numbers n and $\mathbf{k}$ is at all occupied single-electron levels. And $\Omega_{FBZ} = \frac{(2\pi)^3}{\Omega_c}$ where Ω_c is the volume of the unit cell, described as $\Omega_c = \frac{\Omega}{N}$ (the total volume of the crystal (Ω) divided by the number of crystal cells (N).

- The effective potential is:

$$\hat{v}_{eff}[\rho] = \hat{v}_H[\rho] + \hat{v}_{xc}[\rho] + \hat{v}_{ec} \tag{1.56}$$

  The screening potential is:

$$\hat{v}_{scr}[\rho] = \hat{v}_H[\rho] + \hat{v}_{xc}[\rho] \tag{1.57}$$

  So we can so we can consider the effective potential as a screened potential:

$$\hat{v}_{eff}[\rho] = \hat{v}_{scr}[\rho] + \hat{v}_{ec} \tag{1.58}$$

Where we have plane waves in the cristalline momentum basis (using Dirac notation):

$$\xi_{\mathbf{k}}(\mathbf{r}) = \langle \mathbf{r}|\mathbf{k}\rangle = \frac{1}{\sqrt{\Omega}} e^{i\mathbf{kr}} \quad \text{and} \quad \xi_{\mathbf{k}+\mathbf{G}}(\mathbf{r}) = \langle \mathbf{r}|\mathbf{k}+\mathbf{G}\rangle = \frac{1}{\sqrt{\Omega}} e^{i(\mathbf{k}+\mathbf{G})\mathbf{r}} \tag{1.59}$$

The plane waves are orthogonal with each other:

$$\langle \mathbf{k}+\mathbf{G}'|\mathbf{k}+\mathbf{G}\rangle = \frac{1}{\Omega} \int_{\Omega} d\mathbf{r} e^{-i(\mathbf{k}+\mathbf{G}')\mathbf{r}} e^{i(\mathbf{k}+\mathbf{G})\mathbf{r}} = \int_{\Omega} d\mathbf{r} e^{i(\mathbf{G}-\mathbf{G}')} = \Omega\delta(\mathbf{G},\mathbf{G}') \tag{1.60}$$

This is important when calculating the normalisation coefficient and understanding the Ω factor that will appear in multiple expressions.

So the Kohn-Sham orbitals (1.54) can be represented on the basis of crystalline momentum:

$$\phi_{n,\mathbf{k}}(\mathbf{r}) = e^{i\mathbf{kr}} u_{n,\mathbf{k}}(\mathbf{r}) = e^{i\mathbf{kr}} \sum_{\mathbf{G}} c_{n,\mathbf{G}}(\mathbf{k}) \frac{1}{\sqrt{\Omega}} e^{i\mathbf{Gr}} = \sum_{\mathbf{G}} c_{n,\mathbf{G}}(\mathbf{k}) \frac{1}{\sqrt{\Omega}} e^{i(\mathbf{k}+\mathbf{G})\mathbf{r}} \tag{1.61}$$

Using this set of plane wave and the Fourier transform theory, we can act on every single function in both sides (both spaces: direct and reciprocal) as:

$$f(\mathbf{r}) = \sum_{\mathbf{G}} f(\mathbf{G}) e^{i\mathbf{Gr}} \quad f(\mathbf{G}) = \frac{1}{\Omega} \int f(\mathbf{r}) e^{-i\mathbf{Gr}} d\mathbf{r} \tag{1.62}$$

The formalism is well covered in [8], the matrix elements of the generators that appear in the Kohn-Sham equations are:

$$\langle \mathbf{k}+\mathbf{G}|\hat{O}|\mathbf{k}+\mathbf{G}'\rangle = \langle \mathbf{k}+\mathbf{G}|\mathbb{1}\hat{O}\mathbb{1}|\mathbf{k}+\mathbf{G}'\rangle = \tag{1.63}$$

$$= \int\int d\mathbf{r}d\mathbf{r}' \underbrace{\langle \mathbf{k}+\mathbf{G}|r\rangle}_{\frac{1}{\sqrt{\Omega}}e^{-i(\mathbf{k}+\mathbf{G})\mathbf{r}}} \underbrace{\langle \mathbf{r}|\hat{O}|\mathbf{r}'\rangle}_{O(\mathbf{r},\mathbf{r}')} \underbrace{\langle \mathbf{r}'|\mathbf{k}+\mathbf{G}'\rangle}_{\frac{1}{\sqrt{\Omega}}e^{i(\mathbf{k}+\mathbf{G}')\mathbf{r}'}} \tag{1.64}$$

$$\hat{O}(\mathbf{k}+\mathbf{G},\mathbf{k}+\mathbf{G}') = \frac{1}{\Omega}\int\int d\mathbf{r}d\mathbf{r}' e^{-i(\mathbf{k}+\mathbf{G})\mathbf{r}} O(\mathbf{r},\mathbf{r}')\, e^{i(\mathbf{k}+\mathbf{G}')\mathbf{r}'} \tag{1.65}$$

where:

$$O(\mathbf{r},\mathbf{r}') = \int_{\Omega_{FBZ}} d\mathbf{k} \sum_{\mathbf{G},\mathbf{G}'} O(\mathbf{k}+\mathbf{G},\mathbf{k}+\mathbf{G}') e^{i(\mathbf{k}+\mathbf{G})\mathbf{r}} e^{-i(\mathbf{k}+\mathbf{G}')\mathbf{r}'} \tag{1.66}$$

if we have a local operator:

$$O(\mathbf{r},\mathbf{r}') = O(\mathbf{r})\delta(\mathbf{r}-\mathbf{r}') \implies O(\mathbf{k}+\mathbf{G},\mathbf{k}+\mathbf{G}') \equiv O(\mathbf{G}-\mathbf{G}') \tag{1.67}$$

At this moment we know the performance of the basis in all the mathematical objects that we will treat, let us show the result into the Kohn-Sham equations (1.43) changing to a wave-vector dependence. Taking into account the expressions (1.65).

$$\hat{H}\phi_{n,\mathbf{k}}(\mathbf{r}) = \epsilon_{n,\mathbf{k}}\phi_{n,\mathbf{k}}(\mathbf{r}) \implies \sum_{\mathbf{G}'} H_{\mathbf{G}\mathbf{G}'}(\mathbf{k}) c_{n,\mathbf{k}}(\mathbf{G}') = \epsilon_n(\mathbf{k}) c_{n,\mathbf{k}}(\mathbf{G}') \tag{1.68}$$

Where the different matrix terms are:

$$H_{\mathbf{G},\mathbf{G}'}(\mathbf{k}) = \underbrace{\frac{\hbar^2}{2m}|\mathbf{k}+\mathbf{G}|^2 \delta_{\mathbf{G},\mathbf{G}'}}_{\hat{T}_{\mathbf{G}\mathbf{G}'}(\mathbf{k})} + v_{eff}\left(\mathbf{k}+\mathbf{G},\mathbf{k}+\mathbf{G}'\right) \tag{1.69}$$

The kinectic term $\hat{T}_{\mathbf{G}\mathbf{G}'}(\mathbf{k})$ is diagonal, a consequence of the commutation relation between $\hat{H}$ and the traslation operator, that generate as final case that the plane waves are eigenfunctions of the kinetic operator. The operator $V_{eff}\left(\mathbf{k}+\mathbf{G},\mathbf{k}+\mathbf{G}'\right)$ does not depend on $\mathbf{k}$.

$$\rho(\mathbf{G}) = \sum_{n,\mathbf{k}}^{oc} \sum_{\mathbf{G}'} c^*_{n,\mathbf{k}}(\mathbf{G}') c_{n,\mathbf{k}}(\mathbf{G}+\mathbf{G}') \tag{1.70}$$

So far we have not taken into account the shape of the electron-core potential, in our theoretical framework it is possible to apply a pseudopotential scheme such as the one referred to below in the subsection 1.3.10. Due to the spherical harmonic representation, we can treat $\hat{V}_{ec}$ as a sum of a local and a non-local term.

$$\hat{V}_{ec}(\mathbf{r},\mathbf{r}') = \hat{v}^L_{ec}\delta(\mathbf{r}\mathbf{r}') + \Delta\hat{v}^{NL}_{ec}(\mathbf{r},\mathbf{r}') \tag{1.71}$$

Bear in mind the Kohn-Sham (1.43), using the description of the effective potential as it was did in (1.56); also, the local and non-local potential (1.71), finally the Fourier

representation of the different terms (in crystalline momentum representation) are as follows:

- The kinetic term

$$\sum_{n\mathbf{k}}^{oc} \int \phi^*_{n\mathbf{k}}(\mathbf{r}) \left(-\frac{\hbar^2}{2m} \Delta^2 \right) \phi_{n\mathbf{k}}(\mathbf{r}) d\mathbf{r} = \Omega \frac{\hbar^2}{2m} \sum_{n\mathbf{k}} \sum_{\mathbf{G}} |\mathbf{k} + \mathbf{G}|^2 |c_{n\mathbf{k}}(\mathbf{G})|^2 \tag{1.72}$$

- The Hartree term

$$\frac{1}{2} \frac{e^2}{4\pi\epsilon_0} \int \int d\mathbf{r} d\mathbf{r}' \frac{\rho(\mathbf{r})\rho(\mathbf{r}')}{|\mathbf{r} - \mathbf{r}'|} = \Omega \frac{1}{2} \sum_{\mathbf{G}} \rho^*(\mathbf{G}) v_H(\mathbf{G}) = \Omega \frac{1}{2} \frac{e^2}{\epsilon_0} \sum_{\mathbf{G}} \frac{|\rho(\mathbf{G})|^2}{|\mathbf{G}|^2} \tag{1.73}$$

- The exchange-correlation term

$$\int d\mathbf{r} \rho(\mathbf{r}) \epsilon_{xc}(\mathbf{r}) = \Omega \sum_{\mathbf{G}} \rho^*(\mathbf{G}) \epsilon_{xc}(\mathbf{G}) \tag{1.74}$$

- The local-potential term

$$\int d\mathbf{r} \rho(\mathbf{r}) v^L_{ec}(\mathbf{r}) = \Omega \sum_{\mathbf{G}} \rho^*(\mathbf{G}) v^L_{ec}(\mathbf{G}) \tag{1.75}$$

- The non-local potential term

$$\begin{aligned} &\sum_{n\mathbf{k}} \int \int \phi^*_{n\mathbf{k}}(\mathbf{r}') \Delta v^{NL}(\mathbf{r}, \mathbf{r}') \phi_{n\mathbf{k}}(\mathbf{r}) d\mathbf{r} d\mathbf{r}' = \\ &= \Omega \sum_{n\mathbf{k}} \sum_{\mathbf{G},\mathbf{G}'} c^*_{n\mathbf{k}}(\mathbf{G}) c_{n\mathbf{k}}(\mathbf{G}') \Delta v^{NL}_{ec}(\mathbf{k} + \mathbf{G}, \mathbf{k} + \mathbf{G}') \end{aligned} \tag{1.76}$$

- The V_{xc} term

$$\int d\mathbf{r} \rho(\mathbf{r}) v_{xc}(\mathbf{r}) = \Omega \sum_{\mathbf{G}} \rho^*(\mathbf{G}) \left(\epsilon_{xc}(\mathbf{G}) - v_{xc}(\mathbf{G}) \right) \tag{1.77}$$

- The core-core term

$$\frac{1}{2} \frac{e^2}{4\pi\epsilon_0} \sum_{\alpha \neq \beta} \frac{Z_\alpha Z_\beta}{|\mathbf{R}_\alpha - \mathbf{R}_\beta|} \tag{1.78}$$

1.3.10 Pseudopotential Theory

The majority of the pseudopotentials currently used in electronic-structure calculations are generated from all-electron atomic calculations. Within the density functional theory this is done by assuming a spherical harmonics screening approximation and self-consistently solving the radial Kohn-Sham equations [4].

$$\left[-\frac{\hbar^2}{2m}\frac{d^2}{dr^2}+\frac{\hbar^2}{2m}\frac{l(l+1)}{r^2}+V^{AE}\left[\rho^{AE};r\right]\right]rR_{nl}^{AE}(r)=\epsilon_{nl}rR_{nl}^{AE}(r) \tag{1.79}$$

Where:

- Each wavefunction has two parts: $R_{nl}^{AE}(r)$ is the radial part of the wavefunction and $Y_{lm}(\theta,\phi)$ is the angular part of the wavefunction in spherical harmonics.

$$\psi_{nlm}^{AE}=R_{nl}^{AE}(r)\,Y_{lm}(\theta,\phi) \tag{1.80}$$

- The sum of the electron densities associated with the autofunctions of the occupied levels according to the configuration according to the configuration defined by the orbital occupancies f_{nl}.

$$\rho^{AE}=\rho_c^{AE}(r)+\rho_v^{AE}(r)=\sum_{nlm}f_{nl}|\psi_{nlm}^{AE}|^2 \tag{1.81}$$

- $V_H^{AE}\left[\rho^{AE};r\right]$ is the Hartree potential and $V_{xc}^{LDA}\left(\rho^{AE}(r)\right)$ is the local density approximation (1.3.7) for the exhange-correlation potential.

$$V^{AE}\left[\rho^{AE};r\right]=-\frac{e^2}{4\pi\epsilon_0}\frac{Z}{r}+V_H^{AE}\left[\rho^{AE};r\right]+V_{xc}^{LDA}\left(\rho^{AE}(r)\right) \tag{1.82}$$

There are not an unique form to obtain the pseudopotentials but most of them are construted such that they satisfy the following four conditions that Troullier and Martins proposed in [9]:

1. The all-electron and 'pseudo' atom have the same valence eigenvalues for each angular momentum l.
$$\epsilon_l^{PS}=\epsilon_l^{AE}\equiv\epsilon_l \tag{1.83}$$
2. The valence pseudo-wavefuction R_l^{PS} need to be nodeless.
3. The normalized $R_l^{PS}(r)$ is equal to the normalized $R_l^{AE}(r)$ beyond a chosen cut-off radius $r_{core,l}$.
$$R_l^{PS}(r)=R_l^{AE}(r),\quad r>r_{core,l} \tag{1.84}$$
4. Both charges in the sphere with $r_{core,l}$, are identical.
$$\int_0^{r_{core,l}}|R_l^{PS}(r)|^2r^2dr=\int_0^{r_{core,l}}|R_l^{AE}(r)|^2r^2dr \tag{1.85}$$

If a pseudopotential meets the conditions outlined above, it is commonly referred to as a "norm-conserving pseudopotential. Once the pseudo-wave-function is obtained,

the screened (scr) pseudopotential is then recovered by inversion of the radial Kohn-Sham equation (1.79) for the pseudopotential eigenfunctions:

$$\begin{aligned} V_{scr,l}^{PS}(r) &= \frac{\epsilon_l r R_l^{PS}(r)}{r R_l^{PS}(r)} - \frac{\left[-\frac{\hbar^2}{2m}\frac{d^2}{dr^2} + \frac{\hbar^2}{2m}\frac{l(l+1)}{r^2}\right] r R_l^{PS}(r)}{r R_l^{PS}(r)} \\ &= \epsilon_l - \frac{\hbar^2}{2m}\frac{l(l+1)}{r^2} + -\frac{\hbar^2}{2mrR_l^{PS}(r)}\frac{d^2}{dr^2}\left[r R_l^{PS}(r)\right] \end{aligned} \tag{1.86}$$

Kerker made two interesting points in his paper [10] about the consequences of the fact that the wavefunctions are nodeless. There could be a node at the origin but it can be corrected if it behaves in the form r^l; furthermore, the function R_l^{PS} need to be continuous and differentiable at r_{core}.

There is another important thing to note, the expression (1.79) is a second order linear differential equation. Given the screened potential of all the electrons and and energy, the solution of the equation is defined only by the value of the wave function $R^{AE}(r,\epsilon)$ and its derivative $R'^{AE}(r\epsilon)$ at any point $r_{core,l}$.

$$\frac{d}{dr}\ln R^{AE}(r,\epsilon)\Big|_{r=r_0} = \frac{1}{R^{AE}(r,\epsilon)}\frac{dR^{AE}(r,\epsilon)}{dr}\Big|_{r=r_0} \tag{1.87}$$

Finally we put into practice what we have seen in the previous paragraphs, if we take into account the previous 4 conditions, a good expression for R_l^{PS} would be the one proposed by Kerker based on an exponential form using as argument a polynomial of degree 4, the work of Troullier-martins [9] (under a scheme similar to kerker's) works with degree 12.

$$R_l^{PS} = \begin{cases} r^l e^{p(r)} & if \quad r \le r_{c,l} \\ \\ R_l^{AE}(r) & if \quad r \ge r_{c,l} \end{cases} \tag{1.88}$$

Where the function $p(r)$ is defined by:

$$p(r) = c_0 + \sum_{i=2}^{n} c_i r^i \tag{1.89}$$

The c_1 coefficient is not present to avoid a singularity in the pseudopotentials. And our Kohn-Sham equations to solve are (using the expression of the screening potential (1.86) as we saw before):

$$\left[-\frac{\hbar^2}{2m}\frac{d^2}{dr^2} + \frac{\hbar^2}{2m}\frac{l(l+1)}{r^2} + V_{scr,l}^{PS}[\rho^{PS}](r)\right] r^{l+1}e^{p(r)}(r) = \epsilon_{nl} r^{l+1} e^{p(r)} \tag{1.90}$$

If we look at the expression of the screening potential (1.86) , it is determined by the value of R_l^{PS} and its second derivative, we know from the points that it is continuous and differentiable, then we can easily find the value of the potential if we have duly determined its coefficients with the four pre-established conditions.

1.3.11 Hellmann-Feynman Forces

Its interesting to study how can affect directly to the behaviour of different operators the dependency with different continuous parameters. We saw how the equations through this document contains variables such as mass, distance between particles, nucleis. Also the LDA, GGA, pseudopotential theory, ... are influenced by this effects.

Its most common application is the calculation of forces in molecules, where the parameters are the positions of the nuclei, in what is known as molecular mechanics.

Demostration:

Where ψ and H respect, take into account that $|\psi\rangle$ must be normalized and the overlap between different states must be zero:

$$H|\psi\rangle = \lambda|\psi\rangle \tag{1.91}$$

$$\frac{dE}{d\lambda} = \frac{d}{d\lambda}\langle\psi|H|\psi\rangle = \langle\frac{d}{d\lambda}\psi|H|\psi\rangle + \langle\psi|\frac{d}{d\lambda}H|\psi\rangle + \langle\psi|H|\frac{d}{d\lambda}\psi\rangle = \tag{1.92}$$

$$= E_\lambda \underbrace{\left(\langle\frac{d}{d\lambda}\psi|\psi\rangle + \langle\psi|\frac{d}{d\lambda}\psi\rangle\right)}_{\frac{d}{d\lambda}\langle\psi|\psi\rangle} + \langle\psi|\frac{d}{d\lambda}H|\psi\rangle = \langle\psi|H|\psi\rangle \tag{1.93}$$

so, e.g.

$$\frac{dE}{d\mathbf{R}} = \langle\psi|H\left(\mathbf{R},...\right)|\psi\rangle \tag{1.94}$$

In this case, the contributions of this terms only appear in Nuclei-Nuclei interaction and Nuclei-electron. In Density functional theory, actually we have a problem, is not wave-function based. So we need an alternative form. If we remember the Variational principle (1), this theorem actually is a direct consequence.

$$E[\psi[\rho],\lambda] = \frac{\langle\psi[\rho]|H|\psi[\rho]\rangle}{\langle\psi[\rho]|\psi[\rho]\rangle} = E \qquad \left.\frac{\delta E[\psi[\rho],\lambda]}{\delta\psi[\rho]}\right|_{\psi[\rho]} = \psi[\rho]_\lambda = 0 \tag{1.95}$$

Differentiating using the chain rule:

$$\frac{dE}{d\lambda} = \frac{\delta E[\psi[\rho]}{\delta\lambda} + \underbrace{\int \frac{\delta E[\psi[\rho],\lambda]}{\delta\psi[\rho]}\frac{d\psi[\rho]}{d\lambda}dx}_{=0\ (1.95)} \tag{1.96}$$

1.3.12 Birch–Murnaghan isothermal equation of state

In this work we will study the unit cell under different volumes, this means in one way or another that it will be under different ranges of pressures. These pressures produce stresses that can be evaluated from the thermodynamic point of view; this will be the starting point of the Birch-Murnaghan approach. Murnaghan in his work (**??**) speaks of the necessity of certain modifications or at least new theories that allow to work in wider ranges of pressures than those allowed by Hooke's law.

We will make use of the theory belonging to the contiuum mechanics, the Eurelian Finite Strain, thus assuming that we will not take into account only those that occur in a transit long enough to invalidate the infinitesimal strain theory. Also, we will make use of the theory belonging to the contiuum mechanics, the eurelian finite strain, thus assuming that we will not take into account only those that occur in a transit long enough to invalidate the infinitesimal strain theory. We will also make use of two assumptions, we will work with the final state of compression as a reference and in turn, that changes are expanded in squared length before and after compression.

If we have a cube of side X_0 (with volume, $V_0 = X_0^3$), if we perform on it a compression (u such that $u < 0$) acquiring a final side X, we will have the following expression:

$$X = X_0 + u \tag{1.97}$$

Earlier we talked about the execution of the difference of squares, then:

$$X^2 - X_0^2 = X^2 - (X - u)^2 = 2Xu - u^2 \tag{1.98}$$

We must bear in mind, that the compression is uniform so we can speak of a linear dependence between the displacement u and the final length X, where the constant of proportionality is c i.e. $u = cX$, that implies our equation (1.98) is now:

$$X^2 - X_0^2 = \left(2c - c^2\right) X^2 \tag{1.99}$$

In the Eulerian description, the finite strain is defined with a second order approximation (see Eulerian-Almansi approximation (quote)), we denote with subindex 'e' in reference to 'Eulerian':

$$\epsilon_e = c - \frac{1}{2}c^2 \tag{1.100}$$

So the expression (1.99) is now:

$$X^2 - X_0^2 = 2\epsilon_e X^2 \tag{1.101}$$

In order to respect the pre-established notation both in the framework of the Eulerian description and of the approximation we will propose later, it is useful to express it in terms of the stretch ratio; in turn, we will already make use of the relation between the initial and final volume:

$$\underbrace{\left(\frac{X_0}{X}\right)^3}_{\text{Stretch ratio}^3} = (1-2\epsilon_e)^{\frac{3}{2}} = \frac{V_0}{V} \tag{1.102}$$

We now clear the desired quantity in order to be able to explain the birch murnaghan approximation, the eurelian finite strain, by making this quantity positive by compression, redefining it as f^e:

$$f_e = -\epsilon_e = \frac{1}{2}\left[\left(\frac{V_0}{V}\right)^{\frac{2}{3}} - 1\right] \tag{1.103}$$

The Birch-Murnaghan equation

Now we can assume that this process occurs at a constant temperature, for example room temperature, and in addition, with a heat source that helps the change to be gradual, slow enough to meet these standards. With this premise, taking into account the helmholt function, the pressure as a function of volume and thus the equation of state. In addition, the helmholtz equation will be approximated by expanding it as a function of the eulerian finite strain:

$$P = -\left(\frac{\partial F}{\partial V}\right)_T \text{ where } F = \sum_j a_j f_e^j \tag{1.104}$$

Reckon with the dependence of F as a function of f_e which is given as $F(V(f_e))$, then we must take into account that the derivative $\frac{\partial F}{\partial f_e}$ makes the first term a_0 zero, we can consider it totally arbitrary.

And when $P = 0$, the eurelian strain will be also zero, so:

$$0 = 0 - a_1\frac{\partial f_e}{\partial V} - 0 - 0 - \ldots \implies a_1 = 0 \tag{1.105}$$

And we are interested only in the third-order terms, so our initial expression (1.104) remains as:

$$P = -2a_2 f_e\left(\frac{\partial f_e}{\partial V}\right)_T - 3a_3 f_e^2\left(\frac{\partial f_e}{\partial V}\right)_T = -\left(2a_2 + 3a_3 f_e\right) f_e\left(\frac{\partial F}{\partial V}\right)_T \tag{1.106}$$

$$P = -\left(2a_2 + 3a_3 f_e\right) f_e\left(\frac{\partial F}{\partial V}\right)_T = -2a_2\left(1 + \frac{3a_3}{2a_2} f_e\right) f_e\left(\frac{\partial F}{\partial V}\right)_T \tag{1.107}$$

In this expression we see how we still do not know the value of both a_2 and a_3, so we will try to rely on other well-defined constants such as the bulk modulus and its derivative with respect to the pressure, which will appear later in the birch-murnaghan equation as important concepts.

We know that the definitions of the Bulk modulus and bulk modulus pressure derivative are:

$$B = -V\left(\frac{\partial P}{\partial V}\right)_T \tag{1.108}$$

$$B' = \left(\frac{\partial B}{\partial P}\right)_T \tag{1.109}$$

So, our plan will be to solve both expressions and then apply the environmental conditions to obtain the constant values that will allow us to obtain a_2 and a_3.

$$B = -V\left(\frac{\partial P}{\partial V}\right)_T = V\left[2a_2 f_e \frac{\partial^2 f_e}{\partial V^2} + 2a_2\left(\frac{\partial f_e}{\partial V}\right)^2 + 3a_3 f_e \frac{\partial^2 f_e}{\partial V^2} + 6a_3\left(\frac{\partial f_e}{\partial V}\right)^2\right] \tag{1.110}$$

Considering these conditions: $P = 0$ i.e. $f_e = 0$; $B = B_0, V = V_0$:

$$B_0 = V_0\left[0 + 2a_2\left(\frac{-1}{3V_0}\right)^2 + 0 + 0\right] = \frac{2a_2}{9V_0} \implies a_2 = K_0 V_0 \frac{9}{2} \tag{1.111}$$

In the same way for B':

$$B' = -1 + 5 - \frac{2}{9B_0V_0}a_3 \implies a_3 = \left(B_0' - 4\right)\frac{9B_0V_0}{2} \tag{1.112}$$

Finally that leads:

$$P(V) = \frac{3B_0}{2}\left[\left(\frac{V}{V_0}\right)^{-\frac{7}{3}} - \left(\frac{V}{V_0}\right)^{-\frac{5}{3}}\right]\left[1 + \frac{3}{4}\left(B_0' - 4\right)\left(\left(\frac{V}{V_0}\right)^{-\frac{2}{3}} - 1\right)\right] \tag{1.113}$$

And integrating respect V:

$$E(V) = E_0 + \frac{9V_0B_0}{16}\left[\left[\left(\frac{V}{V_0}\right)^{-\frac{7}{3}} - 1\right]^3 B_0' + \left[\left(\frac{V}{V_0}\right)^{-\frac{2}{3}} - 1\right]^2\left[6 - 4\left(\frac{V}{V_0}\right)^{-\frac{2}{3}}\right]^3\right] \tag{1.114}$$

Chapter 2

Methodology

2.1 Introduction

The premise to make more affordable and reduction the computational and time complexity of the N-body Hamiltonian is the key, the foregoing chapters review the general density functional framework where the density plays a central role in this way.

The review exposed the suddenly aproximation of the N-body Hamiltonian that leads into a simpler problem, to have grappled with both fundamental theorems (2) (3), obtaining the impresionant Kohn-Sham equations and the mathematical shortcuts chosen by means of the different approaches outlined above (LDA, CGA, PW, OPW and the Pseudopotential method). It is true that there are many more tools, knowledge, methods and theorems to be explored to understand in a better manner the behaviour of this field but we have a good start point to understand how the computational programs work.

Take into consideration that actually exist a lot of computational programs: free (ABINIT, SIESTA, CPMD, Quantum ESPRESSO) or pay-per-license (VASP, pay version of CASTEP and CPMD) some of them have a free version for educational, research purpose.

In this chapter and in this work, the chosen one is VASP (Vienna ab initio Software Package) we will go through the entire process of the simulations, putting special emphasis on their generation procedure and comparing the results with the experiments, when this is possible.

The materials under study will be the most-representative covalent-bonding semiconductors: (in diamond structure) the non-mental Carbon, the metalloids Silicon and Germanium. They are chosen because they are the best examples of how the structure of a system has a huge impact on its properties. We can't forget the well-known natural (in this work without Nitrogen) hardness of the Carbon and it high-thermal properties. And last but not least, the importance in the industry of the Silicon and Germanium being part, e.g. of batteries, solar modules and different stuff.

2.2 Understanding the work space of VASP

In order to perform the calculation we used the Viena ab initio Simulation Package (VASP), created and published by [11], which implements the DFT methodology explained in the previous sections in a scheme of pseudopotentials and a basis of plane waves. First, we are going to explain how to configure a general simulation and what is the configuration chosen in our case.

We have to differentiate four different input files:

- POSCAR: This file contains the lattice geometry and the ionic positions. We introduce the coordinates of the lattice generators a in 3x3 matrix, that will modified by the lattice constant. And the position of the atoms with respect to this basis. Here appear exposed the diamond structure.
- POTCAR: This file contains the pseudopotential for each atomic species of the material. There are different types of pseudopotentials files, depending of the method selected to calculate them. The one which will be used is PAW PBE.
- KPOINTS: This file contains the grid for the Brillouin zone integration, or in general, for solving the Kohn-Sham equations. There are two main options: to introduce the spacing of the mesh and choose a method to create it automatically, or to introduce it manually. The latter is very convenient to calculate the band structure of the material along high symmetry directions once a self-consistent calculation has been performed and we have the ground state charge density.
- INCAR: This file sets the guidelines of the calculation, such as the method used to integrate over the mesh declared in the KPOINTS file, the energy cut-off in the plane wave expansion, the different ways to portrait our calculus (self-consistent, atomic relaxation previous atomic relaxation, calculation of stress and forces, etc). Also we can change the precision, we will work with "PREC=Accurate", take care of chose "High" because this line can modified the energy cuf-off previously wrote in the file.

Not least, there are other files involved in the calculation in a different manner:

- OUTCAR: This file gives completely all the outputs obtained in the VASP calculation, is really important, we can substract all the information required for the results.
- vasprun.xml: Is the same as OUTCAR but in xml format.
- CHGCAR: This file will be used for the calculation of the Density of States and the Band Structure. Contains the change densities and in some cases helps VASP to recycle some calculations improving the next one. This one has an important role for the DFT calculations, the reason is inside the (1.13), because will fit the densities at start for every step, sometimes we will avoid it.

2.3 Setting up of the best parameters for VASP calculations

One of the premises within the ab initio calculations and their researches is to get as accurate results at an as low computational cost as possible.

In the VASP outputs, we can appreciate two problems:

- Basis set incompleteness: The basis set is discrete and incomplete. In some cases when the volume changes, the program needs to add more plane waves. This could generate a lose of smoothness in the output data.
- The cut-off considered in the inputs, for example,we can set the precission in PREC=Med (in the INCAR) the FFT grids are set to $\frac{3}{4}$ of the value that is in principle required for an exact evaluation of $\hat{H}|\phi\rangle$. This introduces small errors, because when the volume changes the FFT grids do change discontinuously

To solve this problems we take into account:

Setup ENCUT: One important thing to remember, however, is the fact that although a plane wave basis set is "nicely behaved" (bigger basis = more accurate result) this is not true for all types of basis sets (Gaussian basis sets are an important example here).

- PREC = HIGH; NSW = 0; IBRION = -1; SIGMA = 0.1 (SIGMA specifies the width of the smearing in eV.); ISMEAR = 0 (Gaussian Smearing, take care with huge values of ENCUT).
- Take into account that the POSCAR file proposes different values for the encut, a minimum and a maximum. Dont work under the minimum. The range of values will be $[300, 600]$.
- Set a constant grid of kpoints, we try 12x12x12 (cubic) and 16x16x8 (hexagonal).

If we find a energy plateau behaviour in this range, we are right to choose some reasonable value of the ENCUT between them. If we will work with other properties in the future, probably will be higher.

Similar as for the kinetic energy cut-off, if you are working with a periodic system you should check the convergence of your k-point set. The need for k-points arises directly from Bloch's theorem (4), which states that in a periodic potential the wave functions have a periodic magnitude, but it says nothing about their phase (since wave functions are complex they possess both a magnitude and a phase). The phase is called "**k**", and we could assume that the phase was also periodic, but with a different period.

In this situation, we choose as cut-off energy 520 [eV] in each case. As mentioned above, for: C, Si, Ge and Sn; in cubic diamond structure, we choose a uniform grid of 12 × 12 × 12. For the hexagonal diamond the grid is 16x16x8 [a]. This means that the

[a] to select the kpoint grid of the lonsdaleite, the aspect ratio c/a must be respected (see B), although a good approximate value can be double, e.g. see the methodology used in [12].

method that generates the grid of the Brillouin zone will take; for example, 12 points along 3 directions of the reciprocal space in the cubic structure; if it was hexagonal, 2 of each directions of k would be different, like in the case of lonsdaleite.

In brief:

- Use a larger plane wave cutoff, probably, setting up at 520eV as we can see in the plots, a good ENCUT value, with an approximate zero slope.
- Use more k-points, set up in 12x12x12 for the cubic diamond or 16x16x8 for the hexagonal diamond, where the stability of the plots is clearly visible.

2.4 Equations of state

The aim of this section is to determine that the Birch-Murnaghan approximation is a good fit for both graphs: Energy-Volume and Pressure-Volume. The third order isothermal Birch-Murnaghan equation of state $P(V)$ is given by (1.113), after integration, the $E(V)$ by (1.114) and the Bulk-modulus $B(0)$ is represented by (1.111). Also, as we can see in (1.112), exist another parameter $B^{'}(0)$.

So we need four parameters to establish the approximation. As it was theorized, it possible to visualized a parabolic behaviour. So we'll try with least square polynomial fit. This means finding the best fitting curve to a given set of points by minimizing the sum of squares. It takes 3 different inputs from the user, namely X, Y, and the polynomial degree; in this case: volume, energy and second degree (2).
We obtain 3 new parameters a, b, c that will be use to approximate the inputs for the Birch-Murnaghan:

- $V_0 = -\frac{b}{2a} = V_{\text{computed}}\left(\min\left\{E_{\text{computed}}\right\}\right)$
- $E_0 = aV_0^2 + bV_0 + c = \min\left\{E_{\text{computed}}\right\}$
- $B_0 = 2aV_0$
- $B_0^{'} = 4$

As we saw in the first and the second item, we need to get the minimum value of the Energy with VASP and it correspondence value of Volume. So the volume will be modified prior to each vasp run, the volume is set with a minus sign to differentiate it from the lattice parameter.

The range of values selected for the volume will be, choosing as a V_{ref} the one collected in [13] (for C), [14] (for Si), [15] (for Ge), [16] (for Sn), [17] (for Lonsdaleite) and calling $delta = 1$, from $V_{ref} - delta$ to $V_{ref} + delta$ with a pace of 0.1.

2.5 Density of States and Electronic Bands

First to obtain the density of states, we must establish two subprocesses with the program written in bash. We proceed as first subprocess to the obtaining of a static calculation for it, we modify in the file INCAR: ISMEAR, LORBIT, NSW, IBRION.

The reason of each modification is:

- **ISMEAR** = -5: The use of the tetrahedron method with Blöchl corrections (use a Γ-centered k-mesh).
- **LORBIT** = 11: DOSCAR and lm-decomposed PROCAR
- **NSW** = 0: NSW gives the number of steps in all ab-initio Molecular Dynamics runs, it has to be supplied therefore, otherwise VASP crashes immediately after having started.
- **IBRION** = -1: Determines how the ions are updated and moved, in this case with this value they wont moved. But NSW outer loops could perform but NSW = 0.

Now we must remove the changes previously made in INCAR and add a new parameter ICHARG:

- **ICHARG** = 11: To obtain the eigenvalues (for band-structure plots) or the vibrational density of states (vDOS) of a given charge density read from CHGCAR. The self-consistent CHGCAR file must be determined beforehand by a fully self-consistent calculation with a k-point grid spanning the entire Brillouin zone.

Also keep the file generated by VASP, CHGCAR (the reason why ICHARG = 11) in order to have the electronic densities already loaded for the next subprocess. To obtain the bandstructure, we need to do the same as we did for the density of states, then change the KPOINTS file with one with the high-symmetric k-points.

In these representations, we have the band structure on the left side and the density of states on the right side. Here the number of bands used in order to elaborate the graphical representations has been limited, as the number of calculated bands is finite and this means that the visualization of the last bands would not be accurate, taking into account the overlapping between bands.

It is also important to note that the origin of the energy is always taken at the maximum of the highest occupied band. There are two carbon atoms in the unit cell of diamond, which means that the origin of energy coincides with the maximum of the fourth valence band.

2.6 Phonon Dispersion

The dispersion relation relates the different energies $E(\mathbf{k})$ of the phonons to their crystal momentum $\mathbf{k}$ of the reciprocal space. To make this possible, we will make use of the dispersion relation $w(\mathbf{k})$ obtained as a result of expressing the force in harmonic representation (as we can see for exampled in this work [18]) and making use of the travelling solution to express the displacements on the lattice.

The phonopy program created and published by [19] is used to obtain the supercell, the force matrix and then the frequency representation based on the high-symmetrical $\mathbf{k}$-points. The reason for its use is due to the ease of operation as well as the versatility in handling the outgoing plots. It can also be used to calculate the band structures, the density of states which will in fact be attached to the phonon dispersion plots. There are other toolkits such as p4vasp that make use of it for the calculation of supercells and for other reasons, so its understanding is useful.

The use of supercells is chosen to ensure that there is no self-interaction of the displaced atom with itself. If this were not the case, the forces and thus the frequencies at the different hypersymmetric points would be affected. If the unit cell is of the order of 10 Angstrom it will not be necessary, in this case it is much lower, also the stability of the phase in question has to be taken into account. In our case, to avoid any kind of mishap, we have chosen to use 2x2x2 supercells for the cubic structure of the diamond and 3x3x1 for the lonsdaleite (hexagonal diamond).

After a single iteration with vasp in the calculations, the file vasprun.xml is subtracted, where we can obtain the force matrix with phonopy. It is a fast process to obtain the forces, the iteration in question in vasp is quite long.

Then, taking into account the forces and creating a file where the hypersymmetric k points are indicated as well as some parameters such as the size of the supercell, we will obtain the graph in which in the process itself the calculations of the density of states will be made.

Chapter 3

Results and Analysis

In this chapter, in the first instance, we will study the convergence of the structure respect to the cutoff energy of the plane wavebasis and different k-points of integration. In order to establish mostly non-fluctuating values in the subsequent vasp files. And will be discussed why we choose certain values and the validity of the plots.

In order to later face the study of the curves of both the P-V equation of state and its respective E-V. Normally in nature, substances are found in those states that have a certain stability given by an energetic minimum, precisely this is what the Birch-Murnaghan approximation, just remember the equations (1.113) (1.114) tries to predict, if we have an expression of analytical nature, we can study it at a mathematical level to predict other physical quantities of interest.

Finalizing with the study of the band structures in addition to the density of states, which will go together in their respective graphs. Examining how the state energies change from one k-point to the next can tell us useful things such as if a material is likely to have a direct or indirect optical gap, for example. For this we need to visualize how the energies of the states vary with k-point, the electronic band structure. The usual way this is done is to plot the band energies along lines between the various high-symmetry k-points in the Brillouin zone

3.1 Set up best parameters

At first, we will study the convergence of the energy with the cutoff energy and the number of integration points chosen on the Brillouin zone (which we will call the integration grid from now on). To put them in the best values to do a correct analysis; normally, later they will remain constant, after the analysis.

When the slope of the curve of the graph reaches a zero value, as we can see in the next plots totally flat for some x-axis value ranges, we can consider that the energy does not vary significantly (establishing a criterion around the millielectronvolt [meV]). We will take the corresponding value of cutoff 'ENCUT' or number of integration '**k**' (as we said before, it references to the crystal momentum) to set up the next calculations and improve the stability of the results. This is the so-called Convergence test.

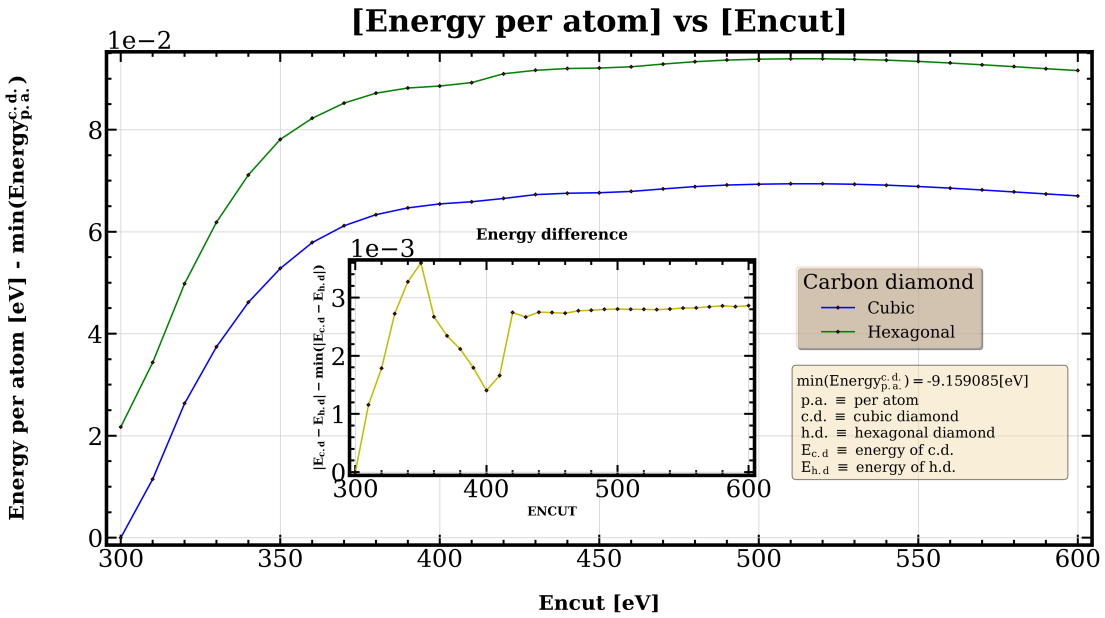

FIGURE 3.1: Energy vs ENCUT (Carbon diamond, cubic vs hexagonal), the kinetic energy cutoff of the plane waves

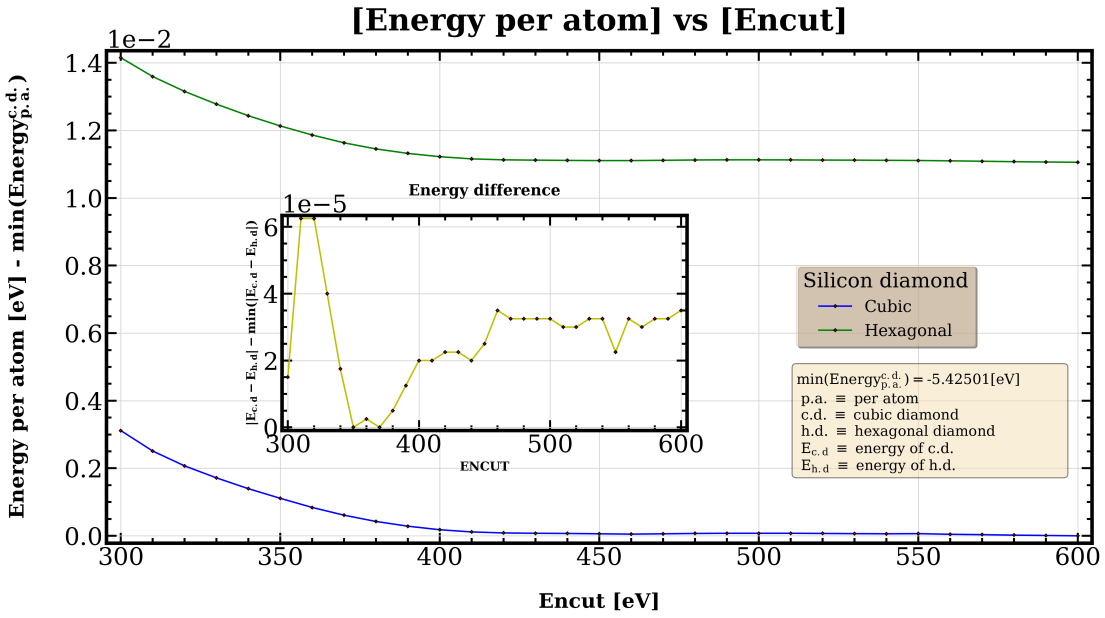

FIGURE 3.2: Energy vs ENCUT (Silicon diamond, cubic vs hexagonal)

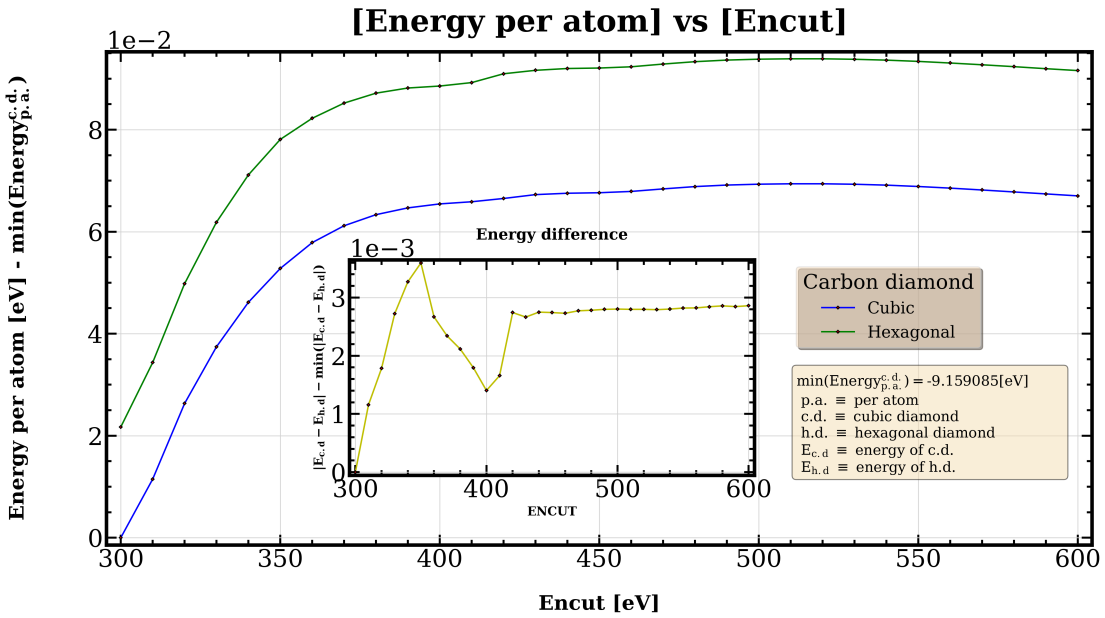

FIGURE 3.3: Energy vs ENCUT
(Germanium diamond, cubic vs hexagonal)

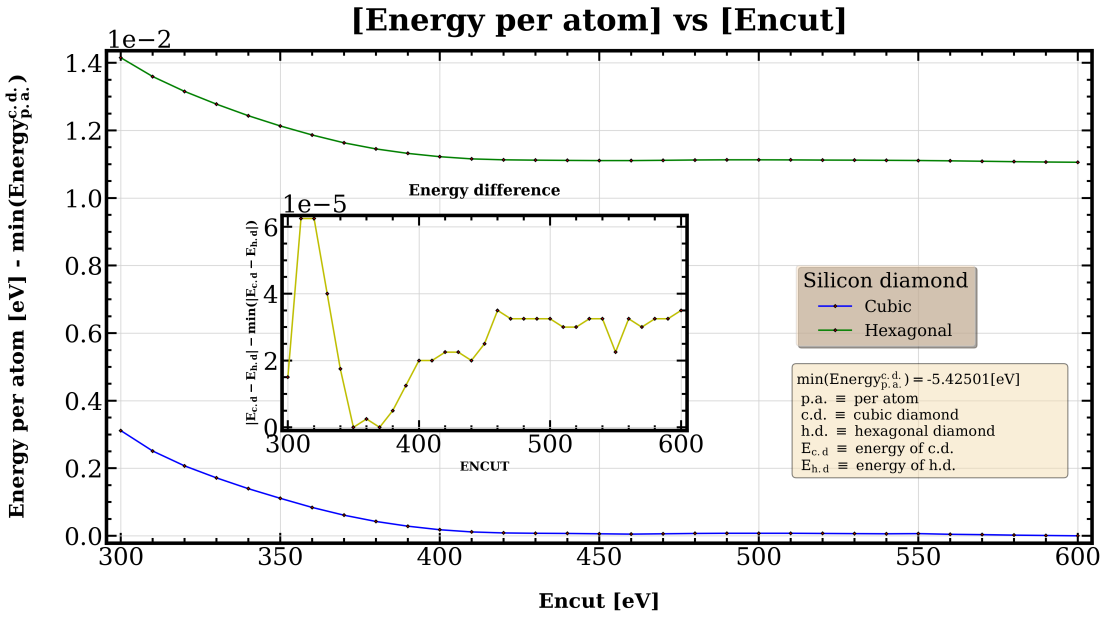

FIGURE 3.4: Energy vs ENCUT (Tin diamond, cubic vs hexagonal)

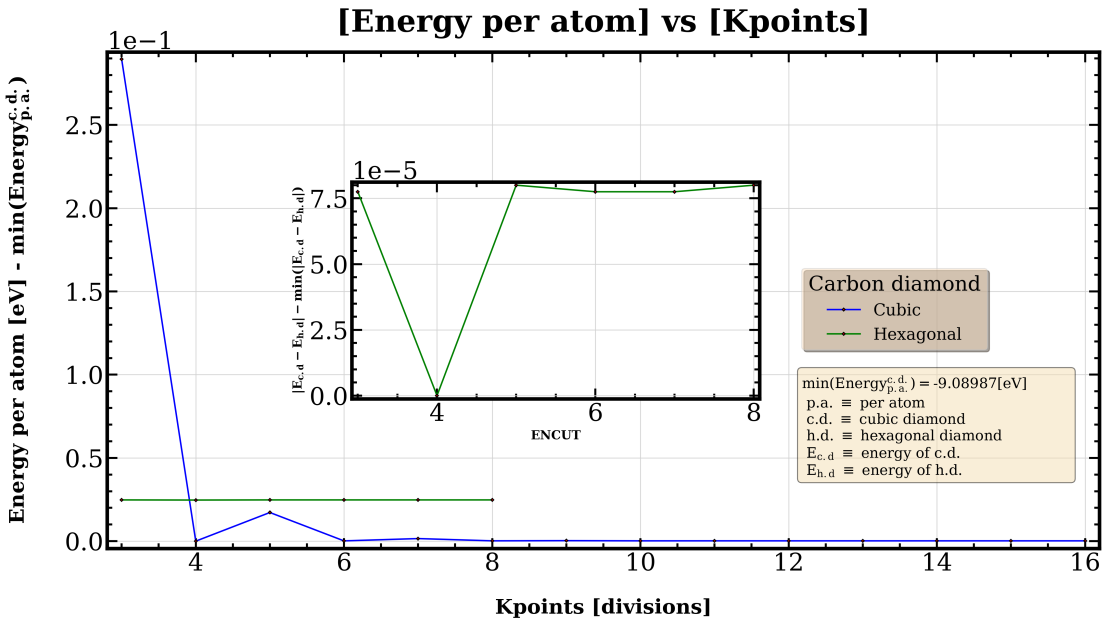

FIGURE 3.5: Energy vs KPOINTS (Carbon diamond, cubic vs hexagonal)

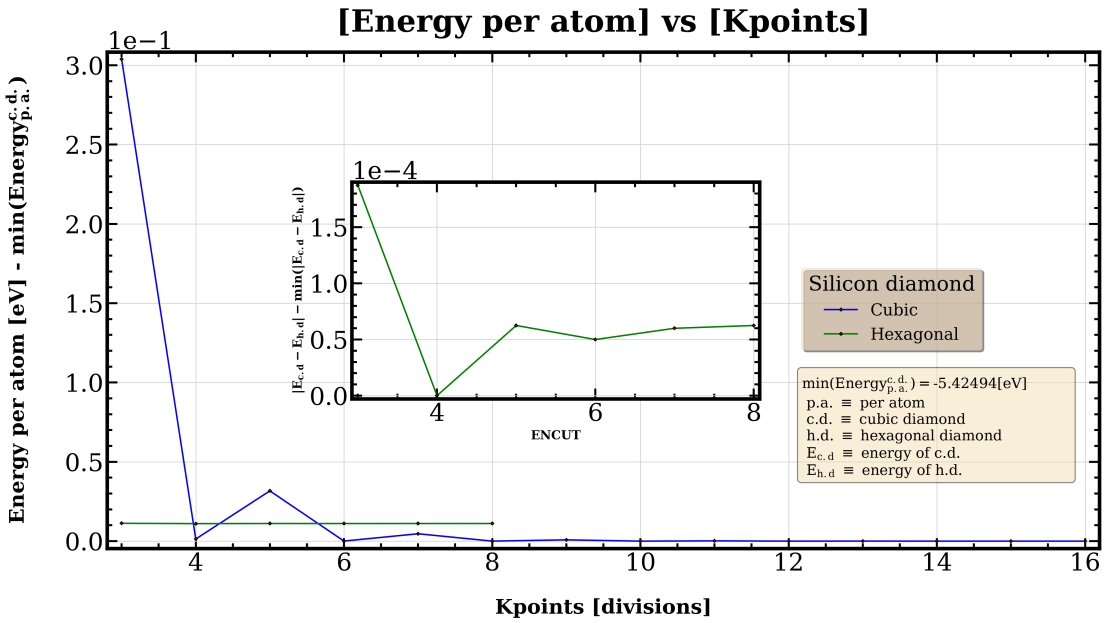

FIGURE 3.6: Energy vs KPOINTS (Silicon diamond, cubic vs hexagonal)

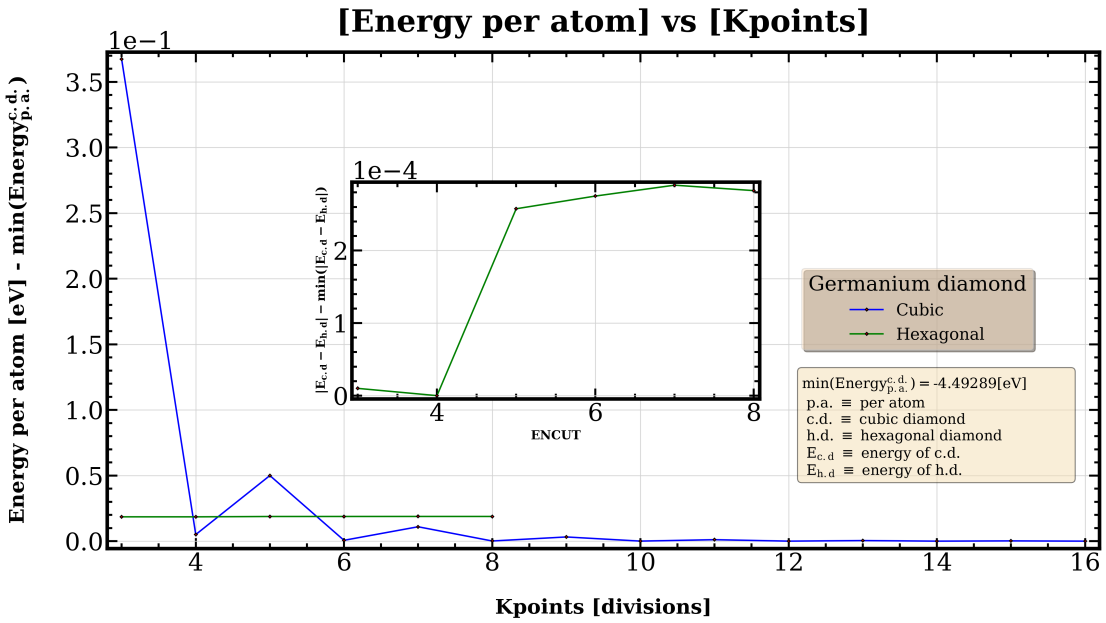

FIGURE 3.7: Energy vs KPOINTS
(Germanium diamond, cubic vs hexagonal)

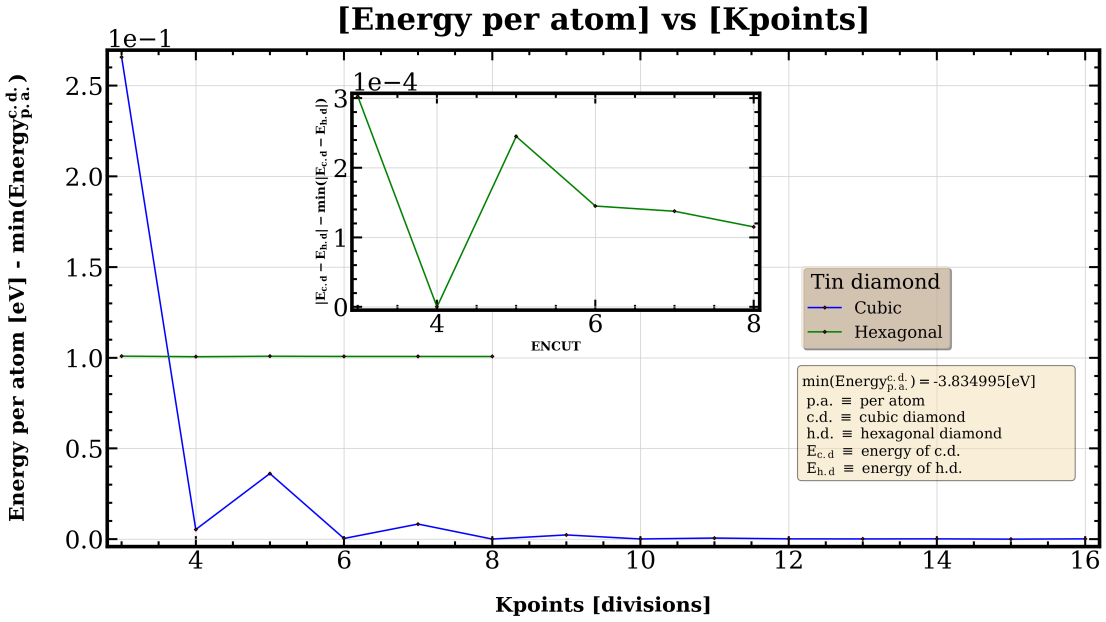

FIGURE 3.8: Energy vs KPOINTS (Tin diamond, cubic vs hexagonal)

In the plots, it can be seen how the curves converge to the order of 1 meV towards an energy value (y-axis), which will be optimal, at least in our work to calculate the subsequent sections. The slope of the energy vs energy of cutoff curve starts to adopt very small values from 450eV, in the energy vs k-poitns of integration curves it happens from the 6x6x6 grid in the case of the cubic diamond structure; however, we see how the oscillations in the curve of the hexagonal structure are minimal, starting from a 6x6x3 grid (in the case of the graph for the point x = 3) visible in 3.1, 3.2, 3.7 and 3.4. This happens because, in the dimensions in which the sides of the cell are equal, the value of kpoint is higher, it coincides even with six, which is the value considered of convergence for cubic diamond, then it places the structure in a good value of convergence from an early value of the grid of KPOINTS.

We can find inside the figures a graph that tries to visualise the difference between the values of the energy for each type of diamond structure, we can see how values of the order of 0.1meV are reached, and also as the atomic number increases, it seems that the difference is somewhat greater.

3.2 Birch-Murnaghan equation of state

The purpose of this subsection is to compare the values obtained by VASP and the Birch-Murnaghan approximation mediated by the quadratic form assumption. Thus, we can obtain the lowest-energy volume. This will be compared with those obtained in different collected papers. As we explained in the section (2.4); for this proposal, the program that we fitted will change the POSCAR archive; in particular, the volume. To calculate the energy relative of each volume associated. Both parameters will be extracted from OUTCAR archive.

The behaviour of the plots that we expect is the same as we saw in the section where we obtain the Birh-Murnugahan equations.

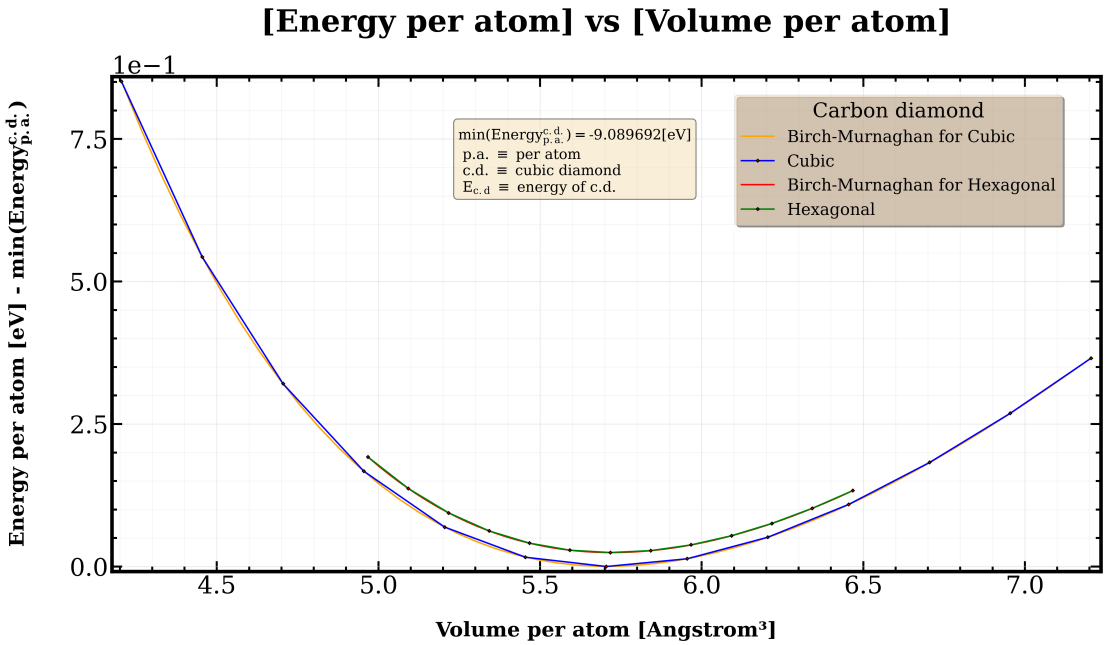

FIGURE 3.9: Energy vs Volume (Carbon diamond, cubic vs hexagonal)

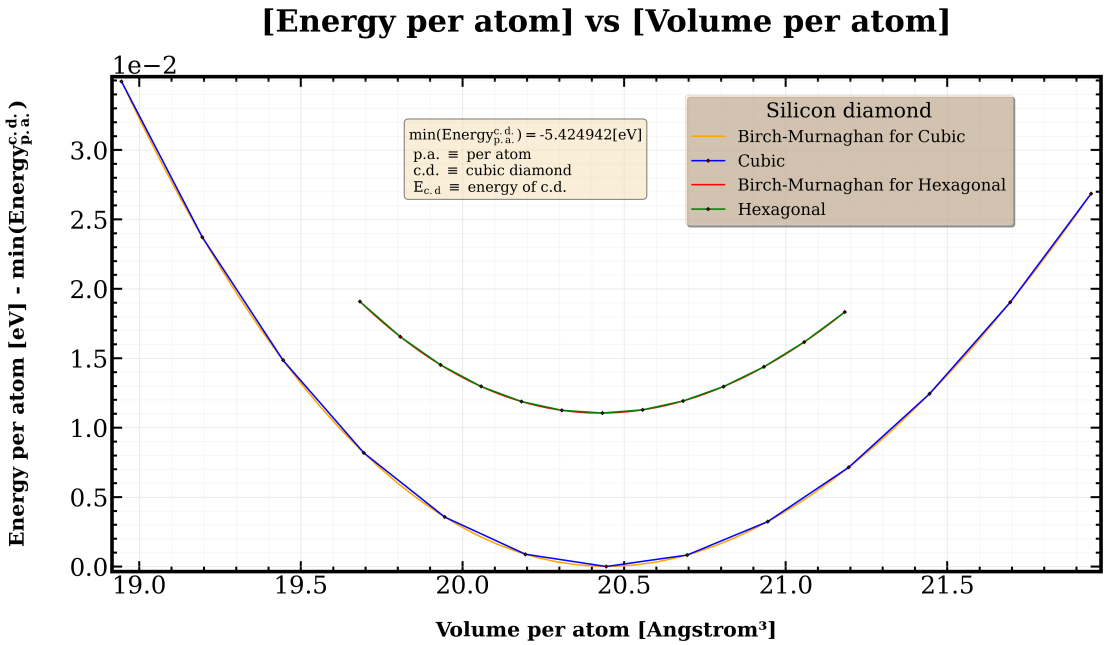

FIGURE 3.10: Energy vs Volume (Silicon diamond, cubic vs hexagonal)

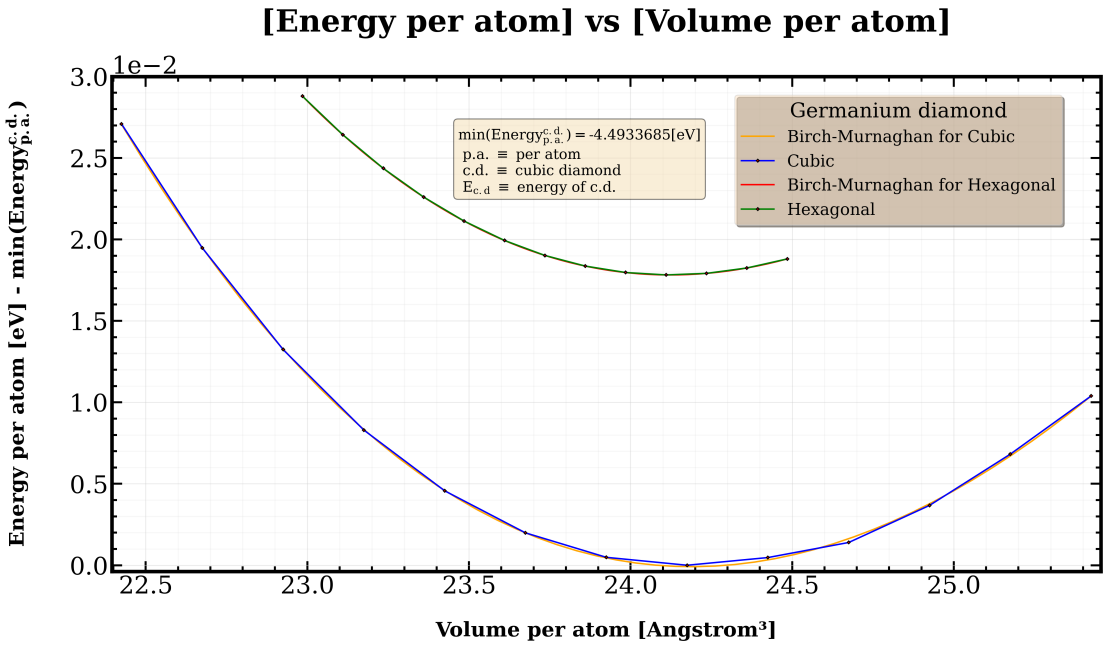

FIGURE 3.11: Energy vs Volume
(Germanium diamond, cubic vs hexagonal)

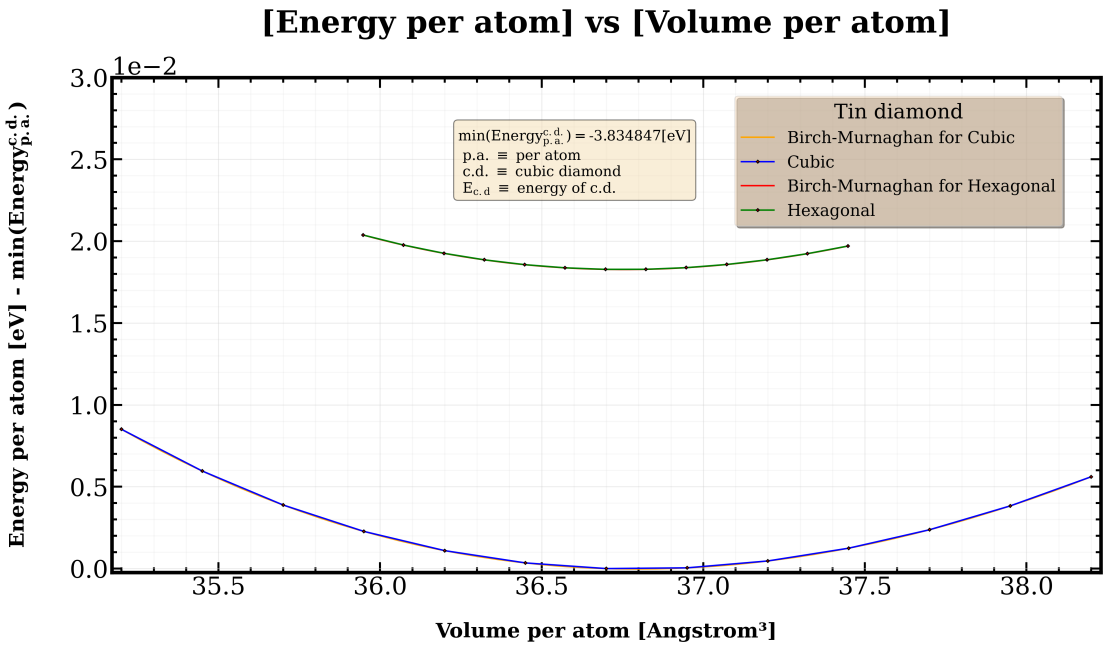

FIGURE 3.12: Energy vs Volume (Tin diamond, cubic vs hexagonal)

We can summarize in two tables the results obtained in the figures [3.9, 3.10, 3.11, 3.12] and comparing these ones with experimental data obtained in different papers, all data shown are rounded to two decimal places:

		Cubic diamond			
		Carbon	Silicon	Germanium	Tin
E_0[eV]	B-M	-9.09	-5.43	-4.49	-3.84
	Published	-	-	-	-
V_0[Å^3]	B-M	5.71	20.45	24.19	36.80
	Published	5.71^b	$18.15^{a,b}$	24.18^b	-
$B_0[GPa]$	B-M	431.40	88.77	58.47	36.25
	Published	435^b	$99.2^{a,b}$	59.2^b	-
$B_0^{'}$	B-M	3.67	4.31	4.79	4.92
	Published	3.51^b	$4.11^{a,b}$	4.6^b	-

TABLE 3.1: Resume table of the comparission between Birch-Murnaghan aproximation, computed data and published data, all for cubic diamond structure, a) [20] b) [21]

.

		Hexagonal diamond			
		Carbon	Silicon	Germanium	Tin
E_0[eV]	B-M	-9.07	-5.41	-4.49	-3.84
	Published	-	-	-	-
V_0[Å^3]	B-M	5.73	20.43	24.12	36.75
	Published	5.722^b	20.43	24.13^b	-
$B_0[GPa]$	B-M	434.06	88.86	59.73	36.53
	Published	434.10^a	87.90^a	55.60^a	-
$B_0^{'}$	B-M	3.67	4.33	4.76	4.83
	Published	3.68^a	4.18^a	4.80^a	-

TABLE 3.2: Resume table of the comparission between Birch-Murnaghan aproximation, computed data and published data all for hexagonal diamond structure, a) [22], b)[21]

From here we can extract some relevant data. The volumes obtained such that they are of minimum energy allow us, taking into account the geometry of the structure, to obtain the associated minimum energy lattice parameter; e.g, for cubic diamond $a_0 = \sqrt[3]{N_{atoms} V_0}$. This quantity is important to understand concepts as the influence of the net parameters in the bandstructure of the crystal.

As we can see in both tables 3.1 and 3.2, the Bulk modulus of the Carbon cubic diamond and the Carbon hexagonal diamond (Lonsdaleite) are similar and higher than the other materials. Since the Bulk modulus implies [23] a higher hardness, it means that in this conditions both materials are harder than the others. Remembering the Bulk modulus is the resistance of the materials to an uniform compression. So one expects expect that the bonds, in a general sense, are weaker for Silicon, Germanium and Tin tan for Carbon.

In general, the coefficient B_0' is overestimated with respect to the works that have been used for comparison. This may be due to several factors, modified POTCAR files (not using exactly the same pseudopotentials), precision by the ENCUT or the chosen KPOINTS, which could be considerably increased in this work, if desired. Even to the Birch-Murnaghan approximation chosen, as we saw that we can perform it in different orders. But mainly is due to using differenct V_{xc} approximations.

The bulk-modulus (in general form) for the case of the cubic structure is underestimated; however, for the case of the hexagonal structure it is overestimated.

The curves shown in the figures for silicon and germanium compared with results as in the [24] work for both cubic structure and lonsdaleite, the volume appears slightly overestimated.

3.3 Electronic bandstructure

At first, we show in B the form of the Brillouin zone as the definition of the points used for represent the electronic bandstructure. So we need to pay attention to the Γ symmetrical point, which is located right in the center of the figure B.2b.

At some distance from Γ, as we saw in the methodology section, we will find the rest of the high-symmetrical points. Then it will help us to locate certain fringes or catalog certain properties around them. We will find different electronic densities loalized to certain energies that will be represented around them.

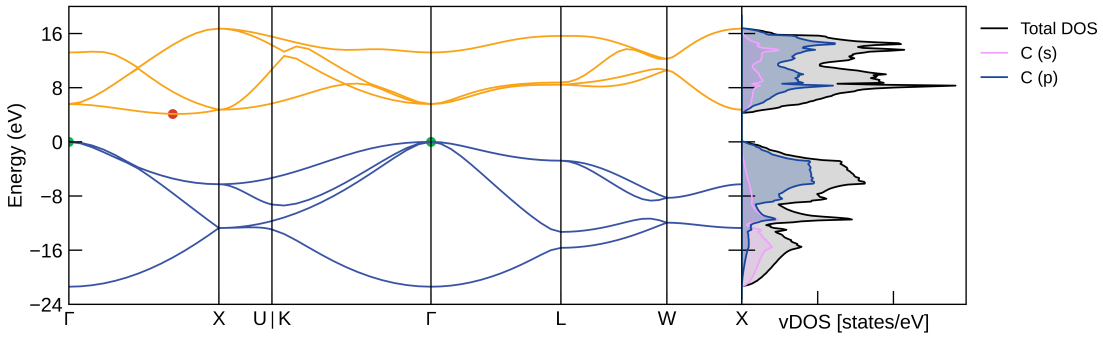

FIGURE 3.13: Bandstructure with vDOS of Carbon cubic diamond

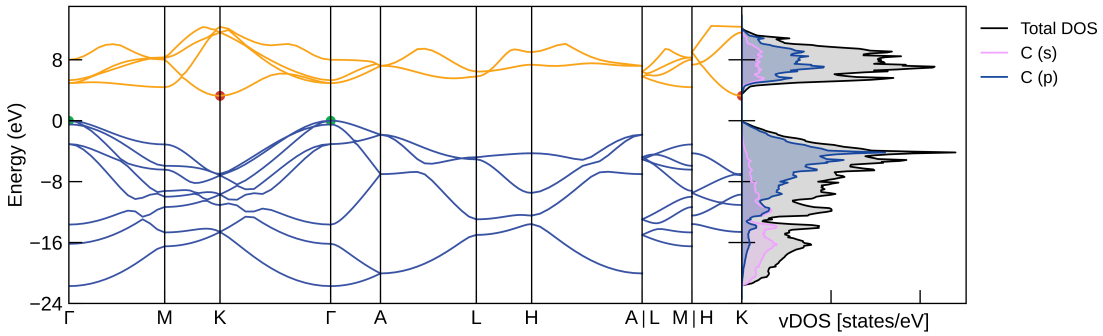

FIGURE 3.14: Bandstructure with vDOS of Carbon Lonsdaleite

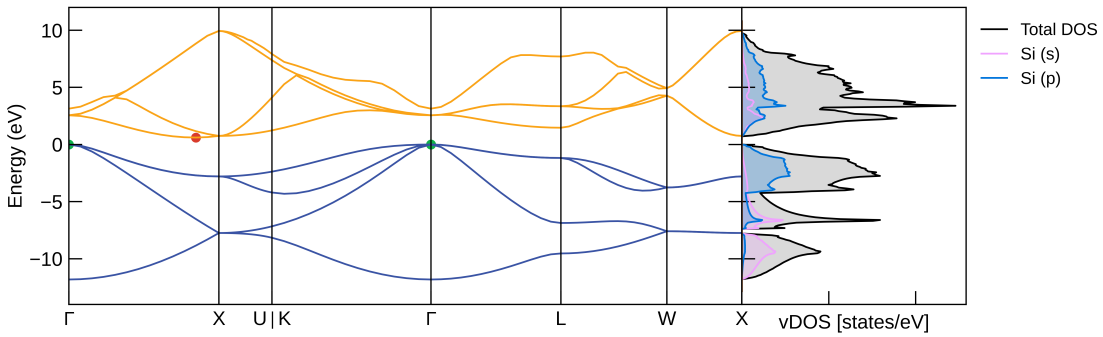

FIGURE 3.15: Bandstructure with vDOS of Silicon cubic diamond

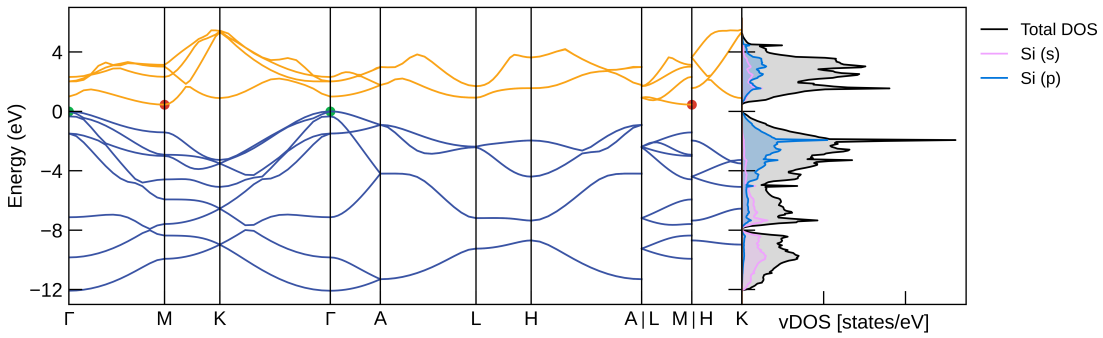

FIGURE 3.16: Bandstructure with vDOS of Silicon Lonsdaleite

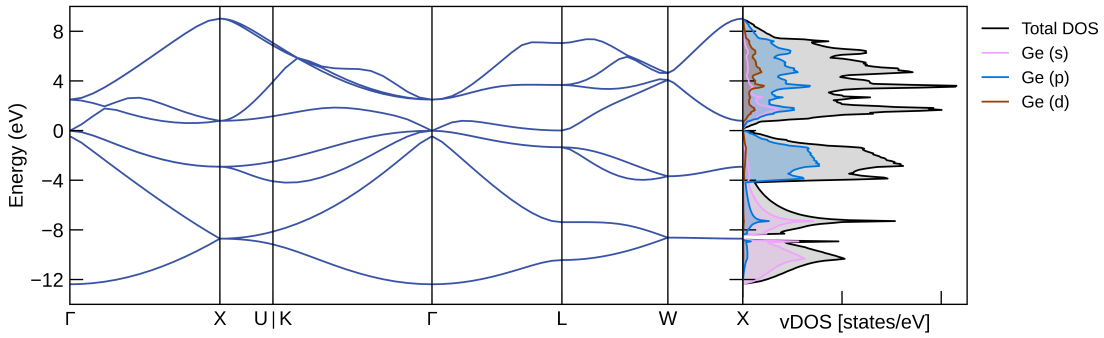

FIGURE 3.17: Bandstructure with vDOS of Germanium cubic diamond

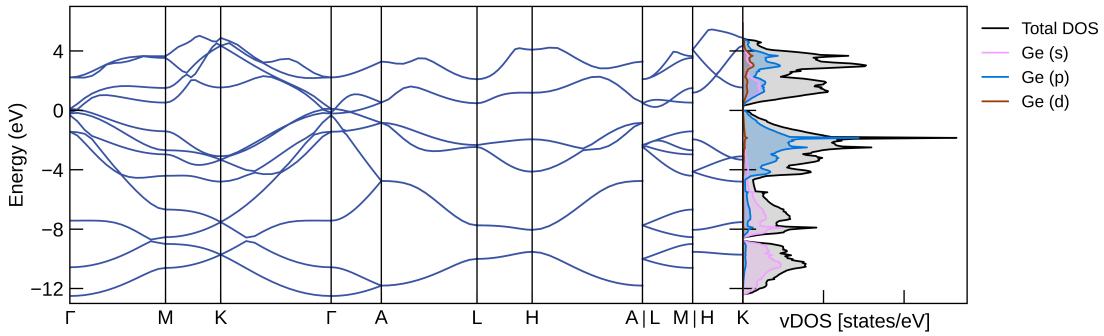

FIGURE 3.18: Bandstructure with vDOS of Germanium Lonsdaleite

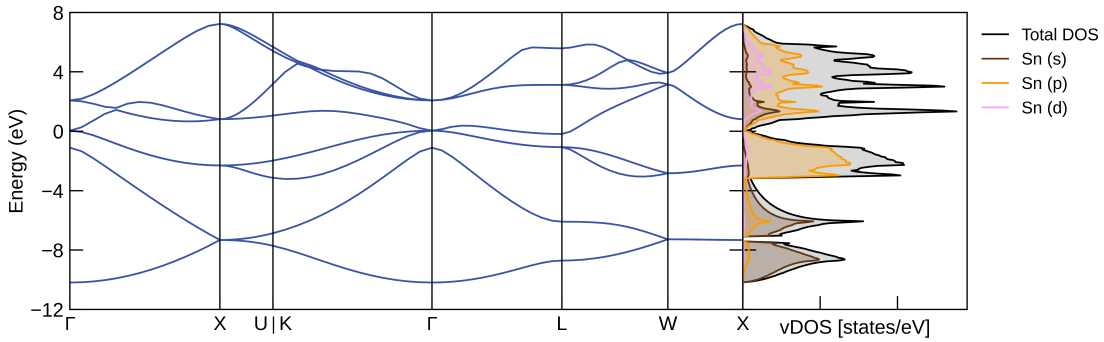

FIGURE 3.19: Bandstructure with vDOS of Tin cubic diamond

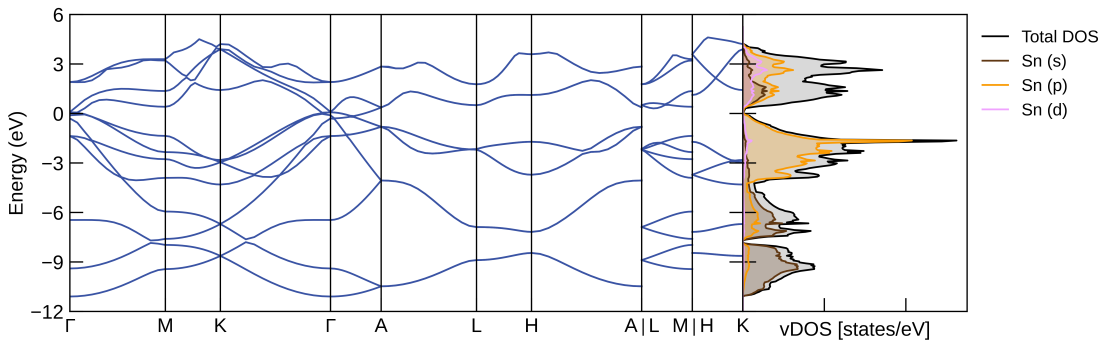

FIGURE 3.20: Bandstructure with vDOS of Tin Lonsdaleite

		Cubic diamond			
		Carbon	Silicon	Germanium	Tin
Computed(c)	$E^{c}_{gap,ind}$ [eV]	4.339	0.731	metallic	metallic
Published(p)	$E^{p}_{gap,ind}$ [eV]	4.339^{a}	0.853^{b}	-	-

TABLE 3.3: Summay table of the different indirect band gaps values
a) [13], b) [14]

		Hexagonal diamond			
		Carbon	Silicon	Germanium	Tin
Computed(c)	$E^{c}_{gap,ind}$ [eV]	4.339	0.998	metallic	metallic
Published(p)	$E^{p}_{gap,ind}$ [eV]	4.339^{a}	0.796^{b}	0.310^{b}	-

TABLE 3.4: Summay table of the different indirect band gaps values
a) [17], b) [25]

In all the figures, in the case of the existence of a bandgap, the conduction bands are marked in yellow and the valence bands in blue, and the maximum of the valence bands are marked in green circles and the minimum of the conductive bands in red.

As we can see in both plots 3.13 and 3.14, is clearly visible a large bandgap that means Carbon and Lonsdaleite are Insulators. The reason why they are insulators is that because the bandgap is so long, the valence band electrons would need a lot of energy to cross these energy levels to access the conduction band, and at low temperatures there is not enough external source for this to happen. The same will not happen in some form or another in semiconductors and metals. We should take into account that the carbon atoms are a priori more electronegative than the others, this causes them to feel more affinity for the electrons, so it is a simple explanation in the first instance of why the bonds appear to be stronger.

In addition, we find that the energy levels associated with this bandgap are not aligned on the same k-vector, they are not both in Γ, the lower boundary of the energy interval is in Γ while the upper boundary is close to the X point. This implies that we are dealing with an indirect bandgap, if the two limits of the interval were at the same k, we would speak of direct bandgap.

In the case of both Germanium 3.17 and Silicon 3.15, we are dealing with two semiconductors, the bandgap is much smaller in relation to that of carbon, it can be clearly seen how the valence and conduction bands are close. It is true that in the graph of Germanium the valence and conduction bands touch at Γ, suggesting that it is a possible conductor or a zero-gap material. In reality, Ge is a semiconductor, but the DFT understimates the band gap and in out calculation it comes out as zero-gap material. One needs to so beyond the DFT to set a band gap for Ge. However, we see in the

corresponding graph of density of states as there is none available for that point hosted in Germanium and with energy 0.

The vDOS is generally lower around the band gap for lonsdaleite, although even lower for silicon 3.16 and germanium 3.18. This is because the conduction bands in e.g. carbon lonsdaleite 3.14 have a minute upward trend; however, in the case of germanium and silicon this is downward, see the work [26].

It is true that in silicon the bandgap is higher, but it is indirect and double in the case of lonsdaleite, taking into account that the symmetrical point path chosen is different.

Already this metallic behavior in Tin 3.19 (in this case α Tin) is also evident, not only because of the nonexistence of a bandgap but also because the domain is uninterrupted in the density of states plot.

Another thing to take into account, entering already in the theory of orbitals is that it is possible to visualize completely the intersection of several bands in the point Γ of the graph of the cubic diamond of carbon 3.13 at energy 0. The orbitals to take into account are $2s^2 2p^2$, there are four electrons in the last energy level, two of them occupying completely the s-type orbital and two occupying the p-type orbital; in addition, we have two atoms per unit cell, this means that there will be 8 valence electrons in total. The free orbitals will be in the conduction band (anti-bonding) while the others will be in the valence band (bonding orbitals). In turn we have sp^3 type hybridizations. The orbitals seen at that point $(\Gamma, 0)$ are p-based ones, even with the hybridization. Here the lower energy S-type is not visible. And the anti-bonding will not be occupied. The same is true for Silicon ($3s^2 3p^2$) and Lonsdaleite. However, the same is not true for Germanium and Tin where the bonding and anti-bonding bands overlap.

The information that has been used in reference to the vDOS has been to make sure that the assumptions made about the type of material in reference to what was seen in the bandstructure plots are met. Also the vDOS plot can show the possible energies allowed for transitions, the probability of this occurring is proportional to the density of states at both the initial and final energy.

We can observe higher maxima in the density of states for negative energies close to zero in the hexagonal structure than in the cubic structure for all cases.

We need to take into acount that normally, the bandgaps will be and are understimated in DFT calculatios in reference to experimental data. Excited electrons cannot be treated with complete ease in DFT with basic but non-trivial approximations such as LDA or GGA, because the bandgap talks about differences of total energies when we know from the Kohn-Sham equations that of the orbitals that are solutions of these equations, they do not really represent the total per se. There are works like [27] that try to solve this problem by means of analytical corrections and at the same time this known understimation of the bandgap. We can see that our results are similar to others obtained by ab-initio calculations, already compared in Tables 3.3 and 3.3. If we also

add these values from the previously mentioned work, we are close to the experimental values.

In both tables 3.3 and 3.3 we can see differences in the values between the cubic carbon diamond and the hexagonal lonsdaleite diamond, certain works like [28] based on those using the Hartree-Fock equations or, as in ours, the DFT theory; Also using VASP and another programs to compare, result in the bandgap of the lonsdaleite always being lower, as has occurred in this case. Another thing that they attest is that the bandgaps other than the indirect minimum that we have already talked about, are closer in the hexagonal structure than in the cubic, something that can also be seen and compared in both figures: 3.13 and 3.14.

Some of the properties that we can deduce from not being able to promote electrons to the anti-bounding bands (established in the conduction bands) are for example the non-coloration of the carbon diamond, in addition to a high resistance to conductivity.

As an indirect gap materials, interband electronic transitions from the maximum of the valence band to the minimum of the conduction band are only possible with the creation of phonons that allow the conservation of the crystalline momentum. In this way, the odds of a phonon being able to make up the difference and conserve momentum is lower so the transition by emitting a photon is much less likely. For this reason this materials can not emit light efficiently.

The points A and H are special points where the energy levels stick together because the structure factor is zero there, see the article [26].

3.4 Phonon Dispersion

The phonon dispersion curves were calculated along several lines of high symmetry. In these crystals, heat is conducted mainly via vibrations.

There are important reasons for this phonon study, because it is important to identify the frequency range, the branches with their modes in order to have a better thermodynamic interpretation in future studies. In analogy to the electronic band structure, phonon dispersion is an important property that directly affects the lattice thermal conductivity of the crystal. When we talk about a thermodynamic interpretation it would be good to emphasize that if we know the frequency behavior (in models like Einstein's, Debye's, ...) we may have calculate the heat capacity.

We will also represent in tables the frequencies with their respective modes in the irreducible representation. The irreducible representation obtained from the application of group theory consists of the representation of the minimum number of components that allows the formation of a group containing all possible combinations of symmetries compatible with the network. It is therefore the representation of the character and the total number of possible vibrations.

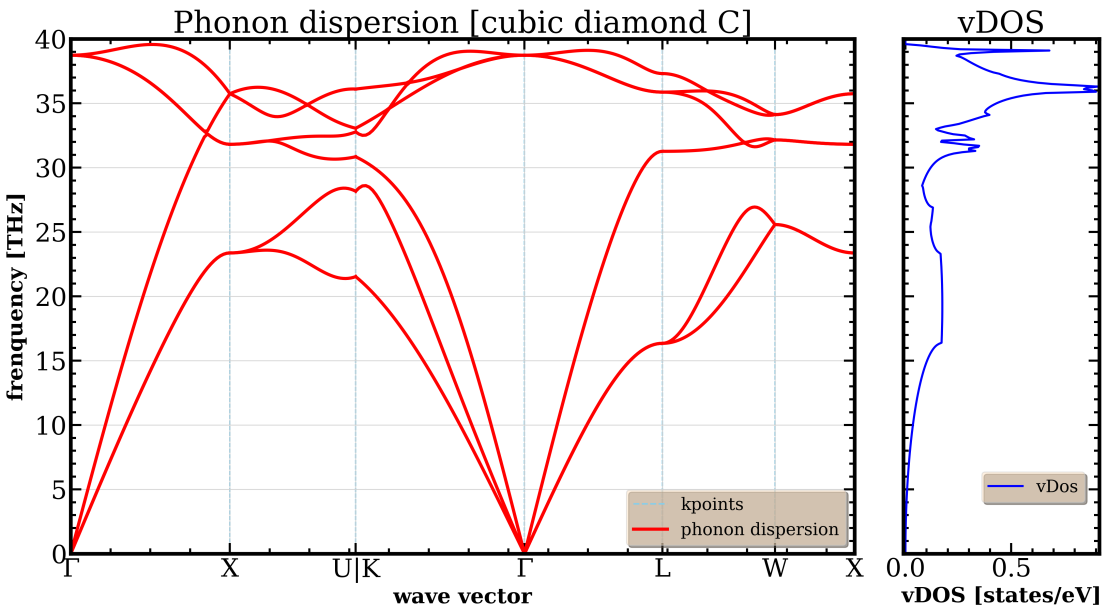

FIGURE 3.21: Plot of the phonon dispersion for Carbon

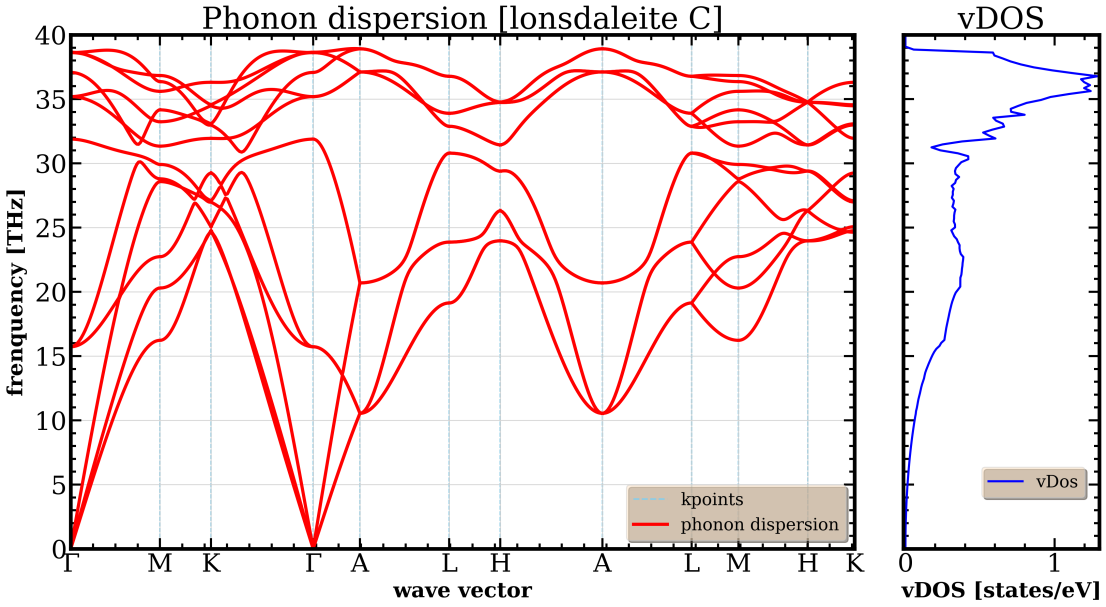

FIGURE 3.22: Plot of the phonon dispersion for Carbon lonsdaleite

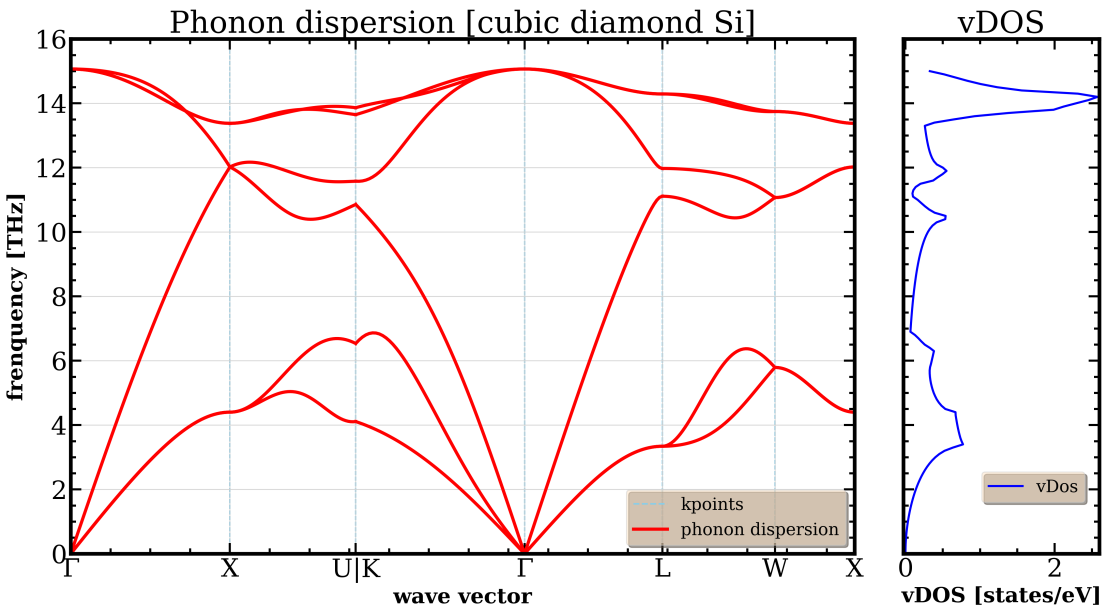

FIGURE 3.23: Plot of the phonon dispersion for Silicon

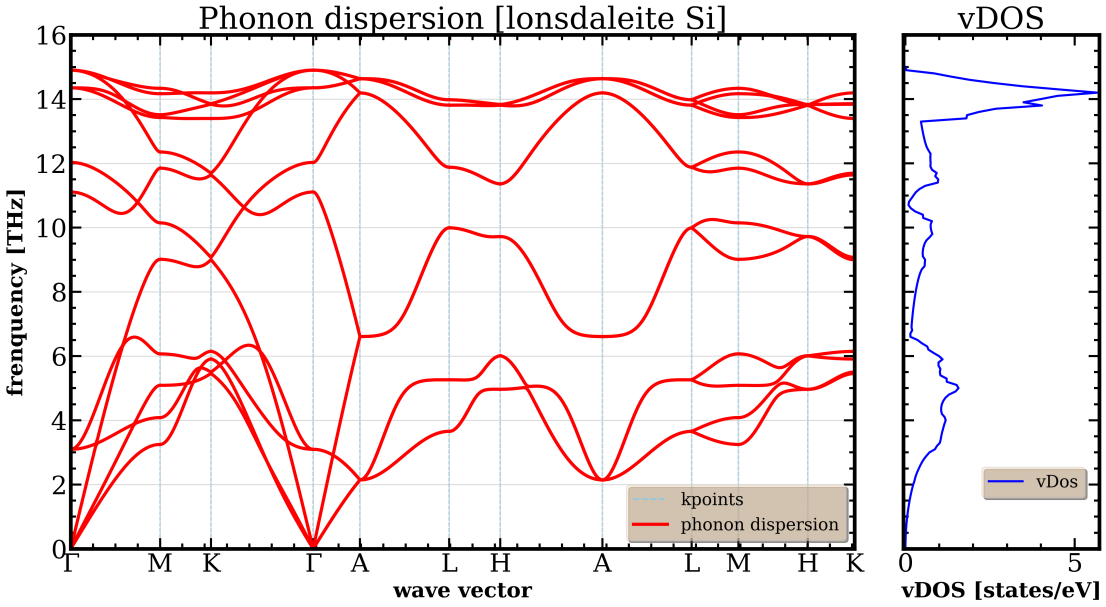

FIGURE 3.24: Plot of the phonon dispersion for Silicon lonsdaleite

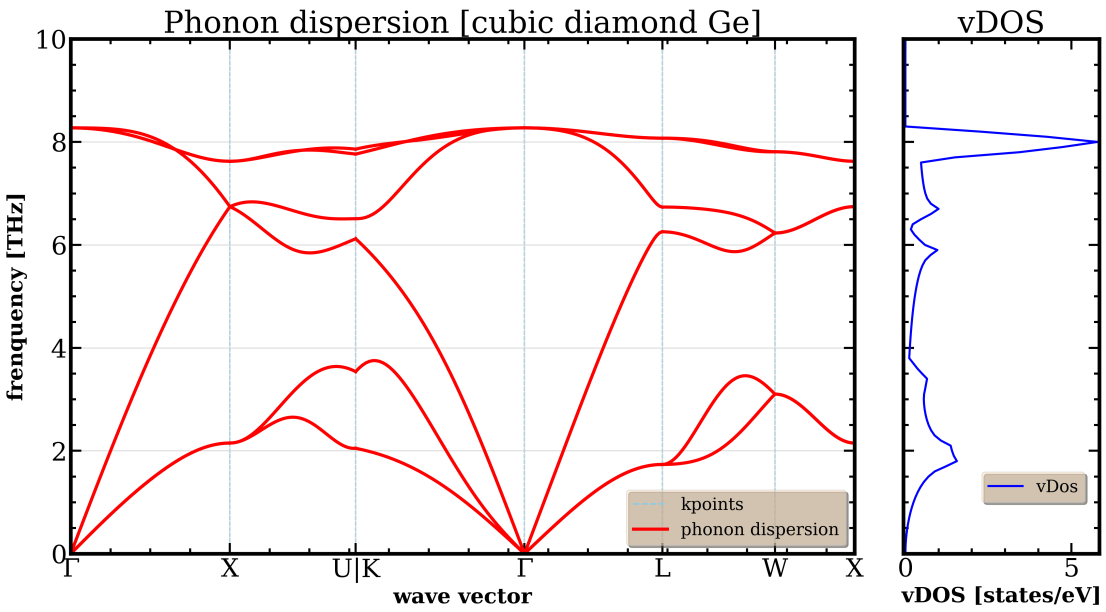

FIGURE 3.25: Plot of the phonon dispersion for Germanium

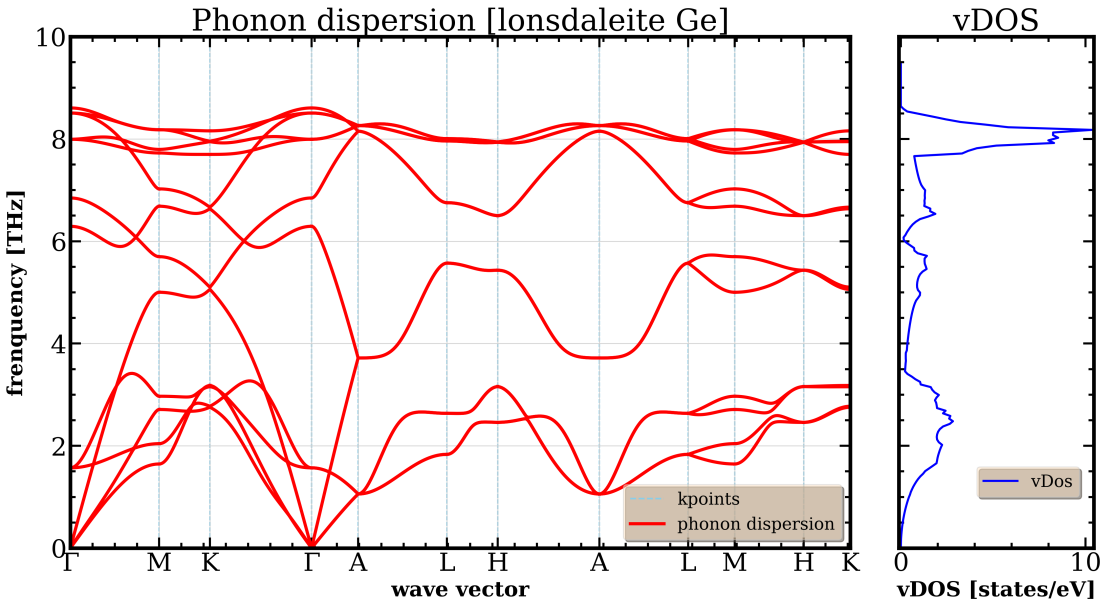

FIGURE 3.26: Plot of the phonon dispersion for Germanium lonsdaleite

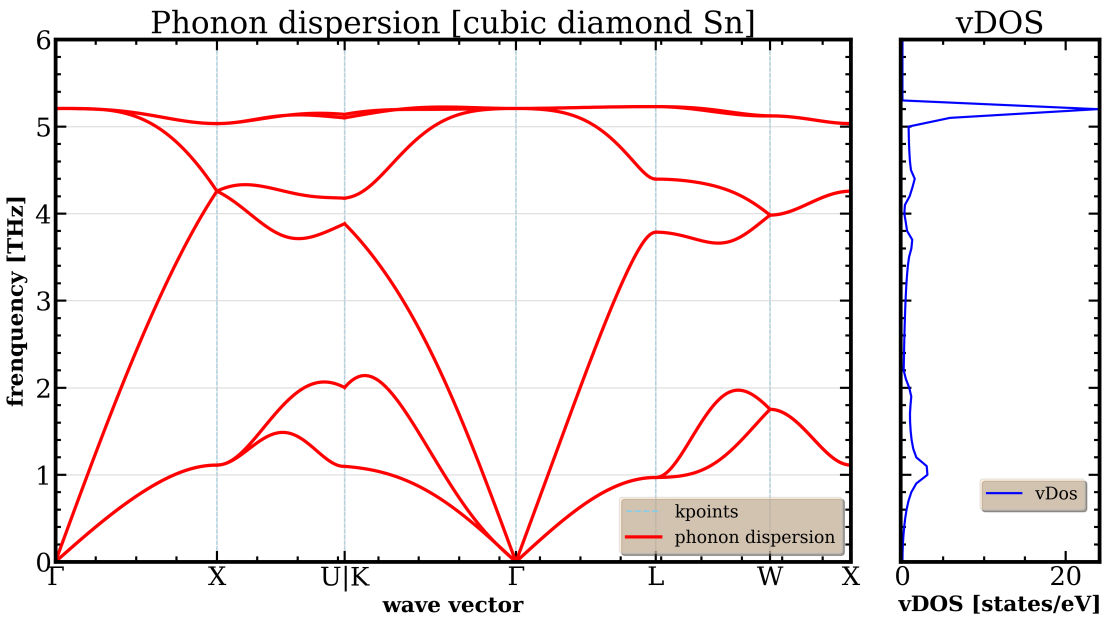

FIGURE 3.27: Plot of the phonon dispersion for Tin

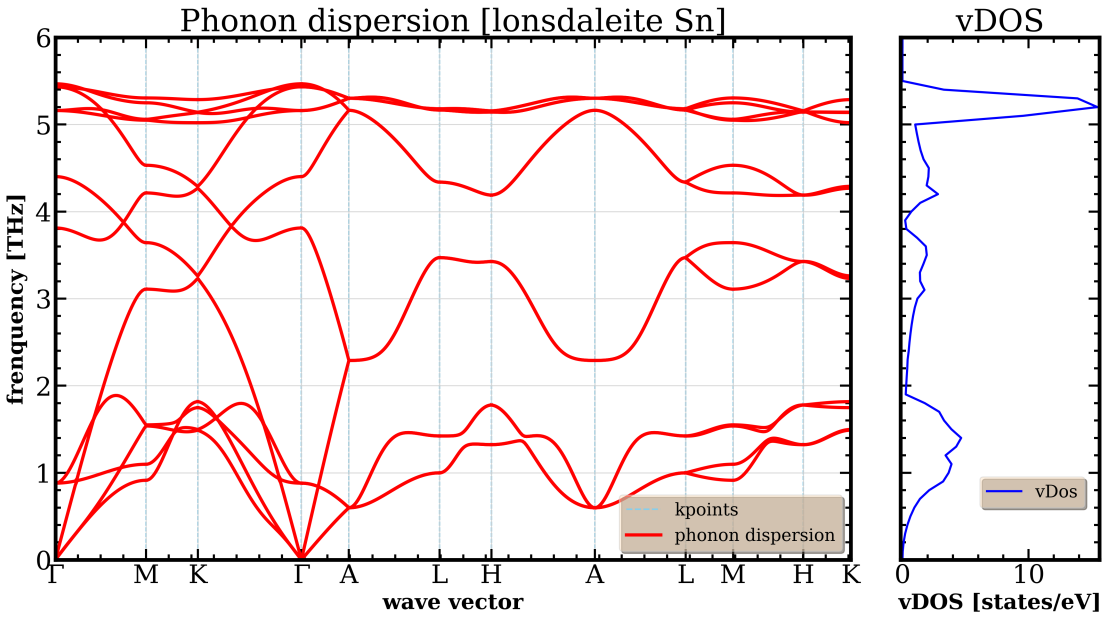

FIGURE 3.28: Plot of the phonon dispersion for Tin lonsdaleite

		frequencies [THz] in cubic diamond			
		Carbon	Silicon	Germanium	Tin
T1u	Γ_4^-	Ac.	Ac.	Ac.	Ac.
T2g	Γ_5^+	38.74	15.07	8.27	5.21

TABLE 3.5: Summary of the frequencies and of the modes at the Γ zone center. "Ac." means Acoustic.

Activity	Character
Infrared	T1u
Raman	T2g
Hyper-Raman	T1u

TABLE 3.6: Summary of the different modes in cubic diamond and their activity.

		frequencies [THz] in hexagonal diamond			
		Carbon	Silicon	Germanium	Tin
E1u	Γ_5^-	Ac	Ac.	Ac.	Ac.
A2u	Γ_2^-	Ac.	Ac.	Ac.	Ac.
E2u	Γ_6^-	15.72	3.10	1.57	0.88
B1g	Γ_3^+	37.07	11.11	6.29	3.81
B2u	Γ_4^-	31.88	12.03	6.85	4.40
E2g	Γ_6^+	35.19	14.35	7.99	5.16
A1g	Γ_1^+	38.65	14.90	8.61	5.47
E1g	Γ_1^+	38.61	14.90	8.51	5.43

TABLE 3.7: Summary of the frequencies and of the modes at the Γ zone center. "Ac." means Acoustic.

Activity	Character
Infrared	A2u + E1u
Raman	A1g + E2g + E1g + B1g
Hyper-Raman	A2u + B2u + E2u + E1u

TABLE 3.8: Summary of the different modes in hexagonal diamond and their activity.

The observation of vibrational modes in crystal is oriented to phonons study, otherwise we can see papers that talk about normal modes in reference of molecules, or at least larger systems than our. As we can see in the plots for Carbon in cubic diamond 3.21 and Lonsdaleite 3.22 the linear dependece of the acoustic nodes near the Γ points is very clear; however, for Silicon 3.23, Germanium 3.25 and Tin 3.27 is good but could be better fitted.

Also, we can see a large number of optical phonon mode for Carbon in cubic and hexagonal diamond but they seem to get flatter as the atomic Z increases as we can see in Ge, Si and Sn. And is clearly visible that both Carbon structures reach higher frequencies than the others, because the bonds in C are much stronger.

For unit cell crystals with two or more atoms (p) per unit cell it is possible to see 3p branches in the dispersion relation. In our cubic diamond case p=2, so we will see 6 branches, 3 acoustic and 3 optical (3p-3). In each type of branch we will see 1 longtudinal and two transverse modes. In the case of lonsdaleite as it has 4 atoms per unit cell, so p=4. Thus we have 3 acoustic and 9 optical.

Some peaks can be glimpsed in the density of states approximated with Gaussians, probably if we increase the number of supercells, some of them would decrease and smooth out. The peaks are related to the stationary points in the bandstructure. In addition, for the vDOS, the $U|K$ point, L and of course in Γ we can appreciate these Van Hove singularities, quite appreciable for Si, Ge and Sn, not so much for Carbon and in Lonsdaleite they are hardly appreciated.

We can also see certain regions that have little dispersion, one in which the dispersion is quite slight, for lonsdaleite in the between the L and H points at a frequency of about 3.2 THz and 4.2 THz, with almost no dispersion between the L and M points, as well as M and H, in which at a frequency of 4.3 THz the curve is completely flat. But this is not true in the same way for all the hexagonal structures, we see how the dispersion is greater in these two zones for carbon and little by little for Si, Ge and Sn this flattening increases.

Common to all the figures is that it is visible how they have resolved upper-frequency phonon bands with very little dispersion resulting in pronounced peaks in the vDOS.

All the profiles seen in the figures are similar, those of the cubic diamond between them and those of the lonsdaleite between them, we can see, however, how carbon has a much higher frequency range, which decreases considerably as the atomic number increases. In the case of lonsdaleite, we see that as the atomic number increases, we see a separation in the curve of the density of states, generating two maxima which continue to separate until the maximum separation given for the tin.

In the table 3.4 , for the carbon cubic diamond, we can find that the found frequency $1292.23cm^{-1}$ (transforming THz into cm^{-1}), although understimated, is similar to the one found in the experimental work with value $1331cm^{-1}$ [29].

Chapter 4

Conclusions

In this work a revision of the basic theory on which the foundations of the Density Functional Theory are based has been carried out. I applied the DFT to the study of the diamond structure of group IV (C, Si, Ge and Sn), in both cases, cubic and hexagonal. The cutoff energy of 520eV and an integration grid for the k-points of 12x12x12 for the cubic structure and 16x16x8 for the hexagonal one have been found as good parameters. A Birch-Murnaghan fitting of the $E(V)$ curve has been obtained, from which the equilibrium volume was obtained. In addition, the band structure and thus the bandgap have been determined quite neatly. Comparison with other investigations shows that the results are plausible. In addition, phonon band structure was obtained which yields certain properties of great interest for any of the elements. The lonsdaleite, understood as an allotrope or as another phase, yields very similar and interesting results in its dispersion curves.

The Vienna ab initio Simulation Package is the program chosen to perform the entire computational block. For a good symbiosis with vasp we made use of the Bash language, to perform operations from the linux shell. And support has been given to subtract different interpretations of the data to Python 3.9 based programs, used in all plots except for the phonon band structure where a Python based program, phonopy, was used.

Appendix A

Basic physics concepts of Solid State Physics

The aim of this chapter is to introduce the basic physics concepts of the solid state physics. Our system is based on a crystallographic structure that has a certain geometry which understanding of this will dictate much of the significant differences of the calculations with respect to other structures, something that will make them unique.

We will talk about how to represent its structure in different reference systems, both Cartesian and reciprocal. How the interior of its structure behaves at the periodic level and how it can be represented mathematically. As well as the internal boundary conditions. It is really a finite system but we will consider it infinite for practical purposes as a theoretical introduction.

A.1 Geometrical understanding about Crystals

A.1.1 Bravais Lattice

We can understand a crystal as a three-dimensional conformation of equal blocks periodically indexed in a three-dimensional space. Then understanding how these blocks are defined as well as their periodic repetition is of utmost importance. Thus, we can establish one of the most important concepts in the description of a crystalline solid, the Bravais lattice, which specifies how the basic components units (atoms, groups of atoms or molecules) are periodically repeated as we talked before.

The physical description of the crystal can be seen as a set of mathematical points repeated, periodically, with an atom (or set) linked in them. The points are the net (lattice) and the atoms the base. Each point is localized via a position vector (in the cartesian 3D space), these points; for example, $\mathbf{r}$ and $\mathbf{r}'$ are related by this expression:

$$\mathbf{r}' = \mathbf{r} + \mathbf{T} \quad \text{where} \quad \mathbf{T} = n_1\mathbf{a_1} + n_2\mathbf{a_2} + n_3\mathbf{a_3} \tag{A.1}$$

Where: $\mathbf{T}$ (traslational vector), $\mathbf{r}$ and $\mathbf{r}' \in \mathbf{R^3}$. The set $\{\mathbf{a_1}, \mathbf{a_2}, \mathbf{a_3}\} \in \mathbf{R^3}$, so-called primitive vectors, are linearly independents and $\{n_1, n_2, n_3\}$ are integers.

This crystalline solid has a volume. As we assume homogeneity, we can represent it by filling it with basic units. Through the study of each of these we can reproduce any

behavior, a priori, of the whole solid. The primitive unit cell contains only one lattice point. We will make use of the primitive vectors (A.1) to describe it mathematically, taking into account that the description does not have to be unique. The primitive vectors will form the edges of a certain primitive cell. All the primitive cells have, with independence of their geometries, the same volume Ω.

An interesting option to choose a primitive cell is the so-called Wigner-Seitz cell. Trace segments from the point of a grid (lattice point) to all of its neighbors, then to plot the bisector planes and the contained volume will be precisely what we are looking for. This type of cell will be used in this work to understand the concept of First Brillouin Zone.

The volume of the primitive cells, either Bravais or Wigner-Seitz, can be obtained as the mixed product of its primitive vectors:

$$\Omega = \mathbf{a_1}(\mathbf{a_2} \times \mathbf{a_3}) \tag{A.2}$$

A.1.2 Reciprocal Lattice

Any physical local property of the crystal has its same traslational invariance. That allows us, for a periodic function like the electron density, to see [30]:

$$n(\mathbf{r} + \mathbf{T}) = n(\mathbf{r}) \tag{A.3}$$

Under these conditions we may consider a Fourier Analysis, the terms allowed to establish the Fourier Space are the points of the reciprocal lattice.

$$n(\mathbf{r}) = \sum_{\mathbf{G}} n_{\mathbf{G}}\, e^{i\mathbf{G}\mathbf{r}} \tag{A.4}$$

Remember that $n(\mathbf{r})$ is not only a real function, is an hermitian operator too. This will be important in next chapter to evaluate the importance of the selection of density as the main variable in this work.

We need to obtain the expression of the vector $\mathbf{G}$ in terms of the Bravais Lattice, that is obtain the set of reciprocal generators $\{\mathbf{b_1}, \mathbf{b_2}, \mathbf{b_3}\}$:

$$\mathbf{b_1} = 2\pi \frac{\mathbf{a_2} \times \mathbf{a_3}}{\Omega} \qquad \mathbf{b_2} = 2\pi \frac{\mathbf{a_3} \times \mathbf{a_1}}{\Omega} \qquad \mathbf{b_3} = 2\pi \frac{\mathbf{a_1} \times \mathbf{a_2}}{\Omega} \tag{A.5}$$

Where $\Omega_{FBZ} = \mathbf{b_1}(\mathbf{b_2} \times \mathbf{b_3}) = \frac{(2\pi)^2}{\Omega}$ (Ω is defined in (A.2)). They have the property:

$$\mathbf{b_i}\mathbf{a_j} = 2\pi\delta_{i,j} \tag{A.6}$$

The reciprocal lattice vectors are $\mathbf{G}$ as:

$$\mathbf{G} = v_1\mathbf{b_1} + v_2\mathbf{b_2} + v_3\mathbf{b_3} \tag{A.7}$$

Where, in tridimensional space: $\mathbf{G}$ (traslational vector in the reciprocal space) $\in \mathbf{R}^{*\mathbf{3}}$. The set $\{\mathbf{b_1}, \mathbf{b_2}, \mathbf{b_3}\} \in \mathbf{R}^{*\mathbf{3}}$, so-called primitive vectors of reciprocal lattice, are linearly independents and $\{v_1, v_2, v_3\}$ are integers. $\mathbf{R}^{*\mathbf{3}}$ in reference to $\mathbf{k}$-space, our reciprocal space.

A.1.3 The First Brillouin Zone (FBZ)

The First Brillouin Zone (FBZ) is the Wigner-Seitz cell of the reciprocal lattice. It is the smallest volume entirely enclosed by planes that are the perpendicular bisectors of the reciprocal lattice vectors drawn from the origin (the property of the Wigner-Seitz that we talked about in last subsection).

These planes and thus their corresponding Wigner-Seitz cell, will be stipulated when mathematically mapping the properties of the diamond structure. And they will be a key point to understand where are the different points in the bandstructure, that will be studied later.

A.1.4 Periodic Potentials & Bloch's Theorem

Drude's model treats the electrons as classical particles making collisions with ions. Then Sommerfeld's model make the assumption that electrons move in an infinite potential well (surfaces of the metals) and Schrodinger equation is solved without considering any potential but only certain boundary conditions.

Since real crystal consists of a periodic array of lattice points or ions, we need to consider the solution of the Schrodinger equation with periodic potential $v(\mathbf{r})$ (A.3) and periodic boundary condition, so we use the expansion (A.4):

$$V(\mathbf{r}+\mathbf{R}) = V(\mathbf{r}) = \underbrace{\sum_{\mathbf{G}} V_{\mathbf{G}} e^{i\mathbf{G}\mathbf{r}}}_{\text{Fourier Series}} \tag{A.8}$$

Theorem 4 (Bloch's Theorem) *The solutions to the Schrödinger equation in a periodic potential take the form of a plane wave modulated by a periodic function.*

$$\psi_{\mathbf{k}}(\mathbf{x}+\mathbf{t_n}) = e^{i\mathbf{k}\mathbf{t_n}} u_{\mathbf{k}}(\mathbf{x}) \tag{A.9}$$

Where $\mathbf{k}$ is the so-called crystalline momentum, $\mathbf{t_n}$ is any traslation or composite of traslations and $u_{\mathbf{k}}(\mathbf{x})$ are periodic. The use of word $\mathbf{x}$ has sense in blibliography, normally in Quantum Mechanics the states are composed by two parts: position and spin, such as $\mathbf{x} = \mathbf{r}\sigma$. We can neglect the spin part in this work so, usually, we will treat $\mathbf{x}$ as $\mathbf{r}$. Is in the book [31].

Proof:

For each Bravais lattice vector $\mathbf{R}$, we define a lattice traslation operator $\hat{T}_{\mathbf{R}}$ and it will shows that commutes with the Hamiltonian :

$$\hat{T}_{\mathbf{R}} f(\mathbf{r}) = f(\mathbf{r}+\mathbf{R}) \tag{A.10}$$

$$\hat{T}_{\mathbf{R}}\hat{H}\psi = \hat{H}(\mathbf{r}+\mathbf{R})\psi(\mathbf{r}+\mathbf{R}) = \hat{H}(\mathbf{r})\psi(\mathbf{r}+\mathbf{R}) = \hat{H}T_{\mathbf{R}}\psi \tag{A.11}$$

That implies:

$$[\hat{H}, \hat{T}_{\mathbf{R}}] = 0 \tag{A.12}$$

$\hat{T}_{\mathbf{R}}$ is a linear operator:

$$\hat{T}_{\mathbf{R}}\hat{T}_{\mathbf{R}'}\psi(\mathbf{r}) = \underbrace{\psi(\mathbf{r}+\mathbf{R}+\mathbf{R}')}_{\text{not order dependency}} = \hat{T}_{\mathbf{R}+\mathbf{R}'}\psi(\mathbf{r}) \tag{A.13}$$

So we can represent the eigenfunctions of the Hamiltonian to be simultaneously eigenstates of the traslation operator via :

$$\hat{T}_{\mathbf{R}}\psi(\mathbf{r}) = c(\mathbf{R})\psi(\mathbf{r}) \tag{A.14}$$

Taking into account that traslation operator is unitary i.e. $\hat{T}_{\mathbf{R}}\hat{T}^{\dagger}_{\mathbf{R}} = \mathbb{1}$ moreover with these properties we can interpret this operator as (remembering equation (A.10) and property (A.14) :

$$\hat{T}_{\mathbf{R}}\hat{T}_{\mathbf{R}'}\psi(\mathbf{r}) = c(\mathbf{R})c(\mathbf{R}')\psi(\mathbf{r}) \tag{A.15}$$

$$\hat{T}_{\mathbf{R}}\hat{T}_{\mathbf{R}'}\psi(\mathbf{r}) = \hat{T}_{\mathbf{R}+\mathbf{R}'}\psi(\mathbf{r}) = c(\mathbf{R}+\mathbf{R}')\psi(\mathbf{r}) \tag{A.16}$$

$c(\mathbf{R})$ has a exponential behavioural as we can see in (A.15) and (A.16), can be expose as: $\hat{T}_{\mathbf{R}} = e^{\hat{f}(\mathbf{R})}$.

$$\text{if } \hat{T}_{\mathbf{R}} = e^{f(\mathbf{R})} \text{ and } c(\mathbf{R}) = e^{i\mathbf{k}\mathbf{R}} \tag{A.17}$$

Finally:

$$\psi(\mathbf{r}+\mathbf{R}) = e^{i\mathbf{k}\mathbf{R}}\psi(\mathbf{r}) \tag{A.18}$$

Born-von Karman boundary condition

The Born-von Karman periodic boundary conditions, explained in the book [31], are important in solid state physics for analyzing many features of crystals, such as diffraction and the band gap. Real solids are confined by surfaces, although we treat them as infinite entities; however, they do possess certain symmetries inside. We impose that:

$$\psi(\mathbf{r}+N_i\mathbf{a_i}) = \psi(\mathbf{r}), \qquad i = 1,2,3 \tag{A.19}$$

Where N_i is the periodicity along $\mathbb{A}_i$ and the relationship $N = N_1 N_2 N_3$ is the total number of primitive cells in the crystal. We can represent [4] such as:

$$e^{i2\pi x_i N_i} = \mathbb{1}, \qquad \mathbf{k} = x_1\mathbf{b_1} + x_2\mathbf{b_2} + x_3\mathbf{b_3}, \qquad \mathbf{k} = \sum_j \underbrace{\frac{m_j}{N_j}}_{x_i} \mathbf{a_j} \tag{A.20}$$

Where m_j are integers. The number of allowed wave vectors in a primitive cell of reciprocal lattice is equal to the total number of lattice sites in the crystal. So,

$$\Delta\mathbf{k} = \frac{\Omega_{FBZ}}{N} = \frac{(2\pi)^3}{N\Omega} = \frac{(2\pi)^3}{V} \tag{A.21}$$

These boundary conditions can be understood as long-range periodic condition, as opposed to the short-range one already explained at the beginning in the symmetry condition (A.3).

Appendix B

Information about diamond structure

B.1 Visualization of structures

(A) Primitive structure (B) Brillouin zone

FIGURE B.1: Both theorical kind of structures of cubic diamond [32]

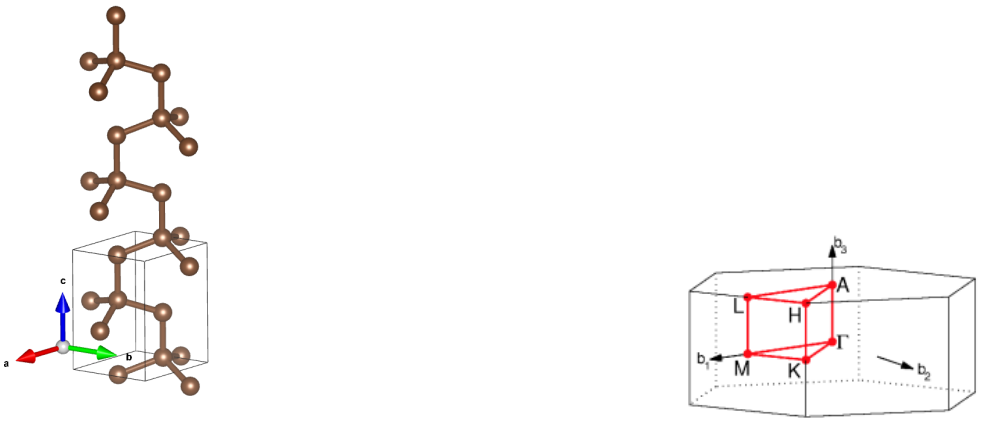

(A) Primitive structure (B) Brillouin zone

FIGURE B.2: Both theorical kind of structures of lonsdaleite [32]

B.2 Cubic diamond structure

For the cubic diamond the following types of atoms in the base are under study:

- C: [He]$2s^2 2p^2$
- Si: [Ne]$3s^2 3p^2$
- Ge: [Ar]$3d^{10} 4s^2 4p^2$
- Sn: [Kr]$4d^{10} 5s^2 5p^2$

The Bravais lattice of the cubic diamond structure (A.1) consists of two basis atoms and may be thought of as two inter-penetrating face centered cubic (FCC) lattices, one displaced from the other, also known as motif, by a translation of $\frac{a_0}{4}(1,1,1)$ along a body diagonal. It belongs to the space group 227(Fd-3m) and point group m3m (Oh), and it holds six 2-fold rotations, four 3-fold rotations, three 4-fold rotations, nine mirror planes and inversion. Where a_0 will denote the lattice constant of the relaxed lattice. Wyckoff Points are 8a.

The primitive vectors , explained in (A.1) for this structure are [33]:

$$\mathbf{a}_1 = \frac{a_0}{2}\begin{pmatrix}0\\1\\1\end{pmatrix} \qquad \mathbf{a}_2 = \frac{a_0}{2}\begin{pmatrix}1\\0\\1\end{pmatrix} \qquad \mathbf{a}_3 = \frac{a_0}{2}\begin{pmatrix}1\\1\\0\end{pmatrix} \tag{B.1}$$

There are two atoms in the basis so in fractional coordinates of the conventional unit, the positions of the two atoms are:

$$\mathbf{A}_2 = \begin{pmatrix}0\\0\\0\end{pmatrix} \qquad \mathbf{A}_2 = \begin{pmatrix}\frac{1}{4}\\\frac{1}{4}\\\frac{1}{4}\end{pmatrix} \tag{B.2}$$

The primitive vectors of the reciprocal lattice are:

$$\mathbf{b}_1 = \frac{2\pi}{a_0}\begin{pmatrix}-1\\1\\1\end{pmatrix} \qquad \mathbf{b}_2 = \frac{2\pi}{a_0}\begin{pmatrix}1\\-1\\1\end{pmatrix} \qquad \mathbf{b}_3 = \frac{2\pi}{a_0}\begin{pmatrix}1\\1\\-1\end{pmatrix} \tag{B.3}$$

B.2.1 Hyper-symmetrical k-vectors of cubic diamond

Here we have the expression of each $\mathbf{k}$:

$$\mathbf{k} = u\mathbf{b}_1 + v\mathbf{b}_2 + w\mathbf{b}_3 \tag{B.4}$$

(u,v,b) are represented by the points:

$$\mathbf{\Gamma} = \begin{pmatrix} 0 \\ 0 \\ 0 \end{pmatrix} \qquad \mathbf{X} = \begin{pmatrix} \frac{1}{2} \\ 0 \\ \frac{1}{2} \end{pmatrix} \qquad \mathbf{L} = \begin{pmatrix} \frac{1}{2} \\ \frac{1}{2} \\ \frac{1}{2} \end{pmatrix} \tag{B.5}$$

$$\mathbf{W} = \begin{pmatrix} \frac{1}{2} \\ \frac{1}{4} \\ \frac{3}{4} \end{pmatrix} \qquad \mathbf{K} = \begin{pmatrix} \frac{3}{8} \\ \frac{3}{8} \\ \frac{3}{4} \end{pmatrix} \qquad \mathbf{U} = \begin{pmatrix} \frac{5}{8} \\ \frac{1}{4} \\ \frac{5}{8} \end{pmatrix} \tag{B.6}$$

Connected via symmetry lines:
Path: $\Gamma \to X \to W \to K \to \Gamma \to L \to U \to W \to L \to K|U \to X$

$$\Lambda : \mathbf{\Gamma} \to \mathbf{L} \qquad \Delta : \mathbf{\Gamma} \to \mathbf{X} \qquad S : \mathbf{X} \to \mathbf{U}, \mathbf{K} \tag{B.7}$$

$$Z : \mathbf{X} \to \mathbf{W} \qquad Q : \mathbf{L} \to \mathbf{W} \qquad \Sigma : \mathbf{\Gamma} \to \mathbf{U}, \mathbf{K} \tag{B.8}$$

B.3 Hexagonal diamond structure

For the hexagonal diamond (lonsdaleite) the following types of atoms in the base are under study:

- C: [He]$2s^2 2p^2$
- Si: [Ne]$3s^2 3p^2$
- Ge: [Ar]$3d^{10} 4s^2 4p^2$
- Sn: [Kr]$4d^{10} 5s^2 5p^2$

The Bravais lattice of the hexagonal diamond structure (A.1) is a hexagonal bravais lattice with 4 basis atoms. It belongs to the space group P63/mmc and point group Fd3m, and it holds 7 point groups that have a single six-fold rotation axis. These 7 point groups have 27 space groups (168 to 194), all of which are assigned to the hexagonal lattice system. [34]. Wyckoff Points are 4f.

The primite vectors are:

$$\mathbf{a}_1 = \frac{a_0}{2} \begin{pmatrix} 1 \\ -\sqrt{3} \\ 0 \end{pmatrix} \qquad \mathbf{a}_2 = \frac{a_0}{2} \begin{pmatrix} 1 \\ +\sqrt{3} \\ 0 \end{pmatrix} \qquad \mathbf{a}_3 = \frac{a_0}{2} \begin{pmatrix} 0 \\ 0 \\ \frac{\sqrt{32}}{3} \end{pmatrix} \tag{B.9}$$

There are four atoms in the basis so in fractional coordinates of the conventional unit, the positions of the two atoms are:

$$\mathbf{A}_1 = \begin{pmatrix} 0 \\ 0 \\ \frac{1}{4} \end{pmatrix} \qquad \mathbf{A}_2 = \begin{pmatrix} 0 \\ 0 \\ \frac{3}{4} \end{pmatrix} \qquad \mathbf{A}_3 = \begin{pmatrix} \frac{2}{3} \\ \frac{1}{3} \\ \frac{1}{4} \end{pmatrix} \qquad \mathbf{A}_4 = \begin{pmatrix} \frac{1}{3} \\ \frac{2}{3} \\ \frac{3}{4} \end{pmatrix} \tag{B.10}$$

The primitive vectors of the reciprocal lattice are:

$$\mathbf{b}_1 = \frac{2\pi}{a_0} \begin{pmatrix} 1 \\ -\frac{1}{\sqrt{3}} \\ 0 \end{pmatrix} \qquad \mathbf{b}_2 = \frac{2\pi}{a_0} \begin{pmatrix} 1 \\ \frac{1}{\sqrt{3}} \\ 0 \end{pmatrix} \qquad \mathbf{b}_3 = \frac{2\pi}{a_0} \begin{pmatrix} 0 \\ 0 \\ \frac{3}{\sqrt{32}} \end{pmatrix} \tag{B.11}$$

B.3.1 Hyper-symmetrical k-vectors of hexagonal diamond

Here we have the expression of each $\mathbf{k}$:

$$\mathbf{k} = u\mathbf{b}_1 + v\mathbf{b}_2 + w\mathbf{b}_3 \tag{B.12}$$

(u,v,b) are represented by the points:

$$\mathbf{\Gamma} = \begin{pmatrix} 0 \\ 0 \\ 0 \end{pmatrix} \qquad \mathbf{A} = \begin{pmatrix} 0 \\ 0 \\ \frac{1}{2} \end{pmatrix} \qquad \mathbf{L} = \begin{pmatrix} \frac{1}{2} \\ 0 \\ \frac{1}{2} \end{pmatrix} \tag{B.13}$$

$$\mathbf{H} = \begin{pmatrix} \frac{1}{3} \\ \frac{1}{3} \\ \frac{1}{2} \end{pmatrix} \qquad \mathbf{K} = \begin{pmatrix} \frac{1}{3} \\ \frac{1}{3} \\ 0 \end{pmatrix} \qquad \mathbf{M} = \begin{pmatrix} \frac{1}{2} \\ 0 \\ 0 \end{pmatrix} \tag{B.14}$$

Connected via symmetry lines:
Path: $\Gamma \to M \to K \to \Gamma \to A \to L \to H \to A|L \to M|K \to H$

$$\Lambda : \mathbf{\Gamma} \to \mathbf{K} \qquad \Delta : \mathbf{\Gamma} \to \mathbf{A} \qquad S : \mathbf{L} \to \mathbf{H} \tag{B.15}$$

$$T : \mathbf{M} \to \mathbf{K} \qquad Q : \mathbf{H} \to \mathbf{A}|\mathbf{L} \qquad \Sigma : \mathbf{\Gamma} \to \mathbf{M} \tag{B.16}$$

$$R : \mathbf{M} \to \mathbf{K} \qquad U : \mathbf{H} \to \mathbf{A}|\mathbf{L} \qquad P : \mathbf{\Gamma} \to \mathbf{M} \tag{B.17}$$

Bibliography

[1] T. E. Bunch, J. H. Wittke, A. West, J. P. Kennett, D. J. Kennett, S. S. Que Hee, W. S. Wolbach, A. Stich, C. Mercer, and J. C. Weaver. Hexagonal Diamonds (Lonsdaleite) Discovered in the K/T Impact Layer in Spain and New Zealand. 2008: PP13C-1476, December 2008.

[2] D. Kraus, A. Ravasio, M. Gauthier, D. O. Gericke, J. Vorberger, S. Frydrych, J. Helfrich, L. B. Fletcher, G. Schaumann, B. Nagler, B. Barbrel, B. Bachmann, E. J. Gamboa, S. Gode, E. Granados, G. Gregori, H. J. Lee, P. Neumayer, W. Schumaker, T. Doppner, R. W. Falcone, S. H. Glenzer, and M. Roth. Nanosecond formation of diamond and lonsdaleite by shock compression of graphite. *Nature Communications*. doi: 10.1038/ncomms10970.

[3] W. Kohn. Nobel lecture: Electronic structure of matter—wave functions and density functionals. *Rev. Mod. Phys.*, 71:1253–1266, Oct 1999. doi: 10.1103/RevModPhys.71.1253. URL https://link.aps.org/doi/10.1103/RevModPhys.71.1253.

[4] P. Hohenberg and W. Kohn. Inhomogeneous electron gas. *Phys. Rev.*, 136:B864–B871, Nov 1964. doi: 10.1103/PhysRev.136.B864. URL https://link.aps.org/doi/10.1103/PhysRev.136.B864.

[5] David A. Mazziotti. Structure of fermionic density matrices: Complete n-representability conditions. *Phys. Rev. Lett.*, 108:263002, Jun 2012. doi: 10.1103/PhysRevLett.108.263002. URL https://link.aps.org/doi/10.1103/PhysRevLett.108.263002.

[6] Timothy J. Giese and Darrin M. York. Density-functional expansion methods: Evaluation of lda, gga, and meta-gga functionals and different integral approximations. *The Journal of Chemical Physics*, 133(24):244107, 2010. doi: 10.1063/1.3515479. URL https://doi.org/10.1063/1.3515479.

[7] Guo-Xu Zhang, Anthony M. Reilly, Alexandre Tkatchenko, and Matthias Scheffler. Performance of various density-functional approximations for cohesive properties of 64 bulk solids. *New Journal of Physics*, 2018.

[8] Andrés Mújica Fernaud. *Estabilidad estructural y polimorfismo en semiconductores IVa y IIIa-Va a alta presión*. PhD thesis, 2000.

[9] N. Troullier and José Luís Martins. Efficient pseudopotentials for plane-wave calculations. *Phys. Rev. B*, 43:1993–2006, Jan 1991. doi: 10.1103/PhysRevB.43.1993. URL https://link.aps.org/doi/10.1103/PhysRevB.43.1993.

[10] G P Kerker. Non-singular atomic pseudopotentials for solid state applications. *Journal of Physics C: Solid State Physics*, 13(9):L189–L194, mar 1980. doi: 10.1088/0022-3719/13/9/004. URL https://doi.org/10.1088/0022-3719/13/9/004.

[11] G. Kresse and J. Furthmüller. Efficient iterative schemes for ab initio total-energy calculations using a plane-wave basis set. *Phys. Rev. B*, 54:11169–11186, Oct 1996. doi: 10.1103/PhysRevB.54.11169. URL https://link.aps.org/doi/10.1103/PhysRevB.54.11169.

[12] Abderrezak Belabbes, Friedhelm Bechstedt, and Silvana Botti. Giant optical oscillator strengths in perturbed hexagonal germanium. *physica status solidi (RRL) – Rapid Research Letters*, 16(4):2100555, 2022. doi: https://doi.org/10.1002/pssr.202100555. URL https://onlinelibrary.wiley.com/doi/abs/10.1002/pssr.202100555.

[13] Kristin Persson. Materials data on c (sg:227) by materials project, Jul 2014.

[14] Kristin Persson. Materials data on si (sg:227) by materials project, Nov 2014.

[15] Kristin Persson. Materials data on ge (sg:227) by materials project, Feb 2016.

[16] Kristin Persson. Materials data on sn (sg:227) by materials project, Feb 2015.

[17] Kristin Persson. Materials data on c (sg:194) by materials project, Jul 2014.

[18] X. Gonze, G.-M Rignanese, and Razvan Caracas. First-principle studies of the lattice dynamics of crystals, and related properties. *Zeitschrift für Kristallographie*, 220:458–472, 05 2005. doi: 10.1524/zkri.220.5.458.65077.

[19] A Togo and I Tanaka. First principles phonon calculations in materials science. *Scr. Mater.*, 108:1–5, Nov 2015.

[20] Tina N Mihm, Tobias Schäfer, Sai Kumar Ramadugu, Laura Weiler, Andreas Grüneis, and James J Shepherd. A shortcut to the thermodynamic limit for quantum many-body calculations of metals. *Nature Computational Science*, 2021. ISSN 2662-8457.

[21] Andrés Mujica, Chris J. Pickard, and Richard J. Needs. Low-energy tetrahedral polymorphs of carbon, silicon, and germanium. *Phys. Rev. B*, 91:214104, Jun 2015. doi: 10.1103/PhysRevB.91.214104. URL https://link.aps.org/doi/10.1103/PhysRevB.91.214104.

[22] S. Wang and H Ye. First-principles study on the lonsdaleite phases of c, si and ge. *Journal of Physics: Condensed Matter*, 15:L197, 03 2003. doi: 10.1088/0953-8984/15/12/102.

[23] J Haines, JM Léger, and G Bocquillon. Synthesis and design of superhard materials. *Annual Review of Materials Research*, 31(1):1–23, 2001. doi: 10.1146/annurev.matsci.31.1.1. URL https://doi.org/10.1146/annurev.matsci.31.1.1.

[24] A Mujica, C J Pickard, and R J Needs. New tetrahedral polymorphs of the group-14 elements. *Journal of Physics: Conference Series*, 950:042010, oct 2017. doi: 10.1088/1742-6596/950/4/042010. URL https://doi.org/10.1088/1742-6596/950/4/042010.

[25] Amrit De and Craig Pryor. Electronic structure and optical properties of si, ge and diamond in the lonsdaleite phase. *Journal of physics. Condensed matter : an Institute of Physics journal*, 26:045801, 01 2014. doi: 10.1088/0953-8984/26/4/045801.

[26] Amrit De and Craig Pryor. Electronic structure and optical properties of si, ge and diamond in the lonsdaleite phase. *Journal of physics. Condensed matter : an Institute of Physics journal*, 26:045801, 01 2014. doi: 10.1088/0953-8984/26/4/045801.

[27] F. Bechstedt and R. Del Sole. Analytical treatment of band-gap underestimates in the local-density approximation. *Phys. Rev. B*, 38:7710–7716, Oct 1988. doi: 10.1103/PhysRevB.38.7710. URL https://link.aps.org/doi/10.1103/PhysRevB.38.7710.

[28] A. S. Barnard, S. P. Russo, and I. K. Snook. Comparative hartree-fock and density-functional theory study of cubic and hexagonal diamond. *Philosophical Magazine B*, 82(17):1767–1776, 2002. doi: 10.1080/13642810208222938. URL https://doi.org/10.1080/13642810208222938.

[29] M. Janák, Nikolaus Froitzheim, Kenta Yoshida, Vlasta Sasinkova, Martin Nosko, T. Kobayashi, T. Hirajima, and Mirijam Vrabec. Diamond in metasedimentary crustal rocks from pohorje, eastern alps: A window to deep continental subduction. *Journal of Metamorphic Geology*, 33, 03 2015. doi: 10.1111/jmg.12130.

[30] C. Kittel. *Introduction to Solid State Physics, 6th edition*. Wiley, New York, 1986.

[31] N. W. Ashcroft and N. D. Mermin. *Solid State Physics*. Holt-Saunders, 1976.

[32] Wahyu Setyawan and Stefano Curtarolo. High-throughput electronic band structure calculations: Challenges and tools. *Computational Materials Science*, (2):299–312, aug 2010. doi: 10.1016/j.commatsci.2010.05.010. URL https://doi.org/10.48550/arXiv.1004.2974.

[33] William Henry Sir Bragg and William Lawrence Sir Bragg. The structure of the diamond. *Proceedings of The Royal Society A: Mathematical, Physical and Engineering Sciences*, 89:277–291.

[34] Akira Yoshiasa, Yu Murai, Osamu Ohtaka, and Tomoo Katsura. Detailed structures of hexagonal diamond (lonsdaleite) and wurtzite-type bn. *Japanese Journal of Applied Physics*, 42(4A):1694–1704, 2003. ISSN 0021-4922. doi: 10.1143/jjap.42.1694. URL https://cir.nii.ac.jp/crid/1390282681234006272.